Patterned Magnetic Nanostructures and Quantized Magnetic Disks

STEPHEN Y. CHOU

Invited Paper

Nanofabrication, offering unprecedented capabilities in the manipulation of material structures and properties, opens up new opportunities for engineering innovative magnetic materials and devices, developing ultra-high-density magnetic storage, and understanding micromagnetics. This paper reviews the recent advances in patterned magnetic nanostructures, a fast-emerging field, including 1) state-of-the-art technology for patterning of magnetic nanostructures as small as 10 nm; 2) engineering of unique magnetic properties (such as domain structures, domain switching, and magnetoresistance) by patterning and controlling the size, shape, spacing, orientation, and compositions of magnetic materials; 3) quantized magnetic disks—a new paradigm for ultra-high-density magnetic storage based on patterned single-domain elements that have demonstrated a storage density of 65 Gb/in^2 (nearly two orders of magnitude higher than that in current commercial magnetic disks) and a capability of 400 Gb/in^2; 4) novel magnetoresistance sensors based on unique properties of magnetic nanostructures; 5) other applications of nanoscale patterning in magnetics such as the quantification of magnetic force microscopy (MFM), and a new ultra-high-resolution MFM tip; and 6) sub-10-nm imprint lithography—a new low-cost, high-throughput technology for manufacturing magnetic nanostructures.

Keywords*—*Magnetic nanostructure, magnetoresistance, nanoimprint lithography, quantized magnetic disk, quantum magnetic disk.

I. Introduction

Magnetic memories and sensors are one of the oldest, yet one of the most widely used, solid-state devices. Already at an annual sale of ~$40 billion, the market is still growing rapidly thanks to the ever-increasing demands in data storage and to new applications of magnetic devices in the field of sensors. New developments and breakthroughs in magnetic materials and devices continue to pour out. Recent examples are giant magnetoresistance (GMR), colossal magnetoresistance (CMR), and nonvolatile magnetic random access memories (MRAM's).

Most magnetic devices used today are based on the properties of thin-film or bulk materials. That is changing drastically, however, due to the advent of nanofabrication technology. Nanofabrication offers unprecedented capabilities in patterning materials with a size smaller than magnetic domain wall, and in manipulating the size, shape, orientation, and composition of the structures. Therefore, nanofabrication allows us to achieve unique magnetic properties that do not exist in a thin-film or bulk material and gives us new freedom in controlling magnetic material properties, leading to innovative magnetic materials and devices, new ultra-high-density magnetic storage, and better understanding of micromagnetics.

This paper reviews recent advances in patterned magnetic nanostructures made at the NanoStructure Laboratory at the University of Minnesota.

II. Brief History

The domain structures in permalloy thin-film bars with an in-plane dimension typically of 10-μm patterned by optical lithography was first studied by Ozimek in 1985 [1], followed by a number of other investigations on the similar structures [2]–[6]. However, only multidomain structures were observed. In 1988, magnetic structures with sub-250-nm feature size patterned by electron beam lithography were reported by two groups. One is from the University of Glasgow, which investigated the magnetic domain structures using transmission electron microscopy (TEM) [7], [8]. The other group is a team of University of California, San Diego (UCSD) and IBM, who studied interaction between the patterned magnetic bars as a function of the bar size and spacing to mimic an interaction between magnetic particles in magnetic tapes [9], [10]. In 1993, the same UCSD and IBM team reported observation of single-domain formation in the patterned bars using magnetic force microscopy (MFM), switching of the bars using a MFM tip, and angle dependence of switching field [11], [12].

Manuscript received September 21, 1996; revised February 10, 1997. This work was supported in part by the Office of Naval Research, Defense Advanced Research Projects Agency, Packard Foundation through a Packard Fellowship, and the Army Research Office through a DURIP.

The author is with the NanoStructure Laboratory, Department of Electrical Engineering, University of Minnesota, Minneapolis, MN 55455 USA.

Publisher Item Identifier S 0018-9219(97)03279-9.

Research on patterned magnetic structures at the NanoStructures Laboratory at the University of Minnesota started in 1991. In a joint study with the micromagnetics group at Minnesota (headed by Prof. Zhu), nanoscale single-domain Ni bars were patterned using electron beam lithography were used as a "point" magnetic charge to deconvolute the true image of a raw MFM image [13]. Later, the NanoStructure Laboratory reported the fabrication and study of Ni bars with a minimum dimension of 15 nm, and proposed a new ultra-high-resolution MFM tip which has a single-domain magnetic spike fabricated on a conventional atomic force microscope (AFM) tip [14]. In 1993, quantized magnetic disks (QMD) based on lithographically patterned magnetic nanostructures were proposed [15], [16], and the fabrication and study of a QMD with a density of 65 Gb/in^2 were reported [17]. To solve the manufacturing problem for QMD's and other patterned magnetic nanostructures, nanoimprint lithography—a low-cost, high-throughput nanofabrication technology, was proposed and demonstrated in 1995 [18], [19].

Another team from Stanford University studied patterned Co and Fe rectangles contributing to early development of pattern magnetic structures [20]–[23].

Since 1995, research in patterned magnetic nanostructure (PMN) has been spreading to spread rapidly due to: 1) application of nanofabrication technology to magnetics; 2) availability of scanning magnetic force microscopy, allowing us for the first time to image and manipulate the magnetic domain structures with great precision; and 3) invention of nanoimprint lithography, a sub-10-nm resolution, high-throughput, low-cost, manufacturing technology that makes commercialization of PMN-based memories and sensors economically viable.

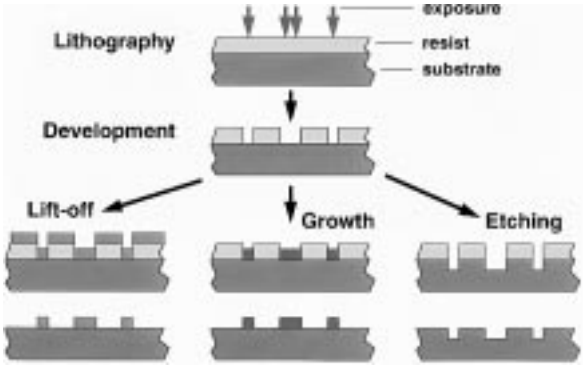

Fig. 1. Schematic of a typical process for fabricating nanomagnetic structures that consists of nanolithography followed by either lift-off, growth, or etching.

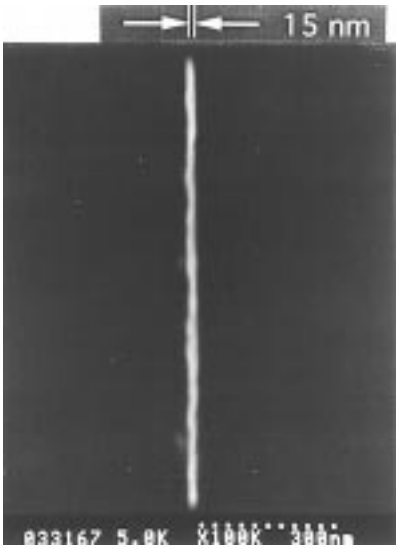

Fig. 2. SEM image of an isolated Ni bar that is 15-nm wide, 1-μm long, and 35-nm thick.

III. Fabrication of Magnetic Structures Using Nanolithography

A typical fabrication process is illustrated in Fig. 1. The first step is to create a resist template. A resist film, such as polymethyl methacrylate (PMMA), is spun onto a substrate, exposed using a lithography tool, such as electron beam lithography, and developed in a cellosolve and methanol solution to form patterns [24]. The resist template can be used to pattern nanostructures using either a lift-off or electroplating process. In a lift-off process, after a ferromagnetic metal film is deposited onto the entire sample, the sample is immersed in acetone which dissolves the PMMA template and lifts off only the metal on the PMMA surface, but not the metal on the substrate. In an electroplating process, a thin metal plating base is placed between the PMMA and the substrate, and the PMMA template is removed after plating. Besides for lift-off and plating, the PMMA template also can be used to etch nanostructures into the substrate, which will be used later to create magnetic nanostructures.

Figs. 2–4 show scanning electron microscope (SEM) images of three magnetic nanostructures fabricated using e-beam lithography and a lift-off process [14], [16]. The nanostructures are an isolated Ni bar 15 nm wide and 1 μm long, an interactive array of 20-nm-wide and 200-nm-long Ni bars, and Ni rings with a 90-nm mean diameter and 25-nm ring width. The Ni structures have a thickness of 35 nm and were fabricated on a Si substrate. Fig. 5 shows an SEM image of a Ni pillar array with 100-nm spacing, 75-nm average diameter, 700-nm height, and therefore a 9.3 aspect ratio fabricated using e-beam lithography and electroplating [17].

IV. Nanoimprint Lithography—Sub-10-nm Feature Size, High-Throughput, Low-Cost Manufacturing Technology

The commercial success of any magnetic storage system relies on low-cost. There is no exception for the PMN-based magnetic storage system. Conventional nanolithography technologies, such as e-beam lithography, X-ray lithography, and scanning probe-based lithography, however, are very expensive, creating a hurtle that must

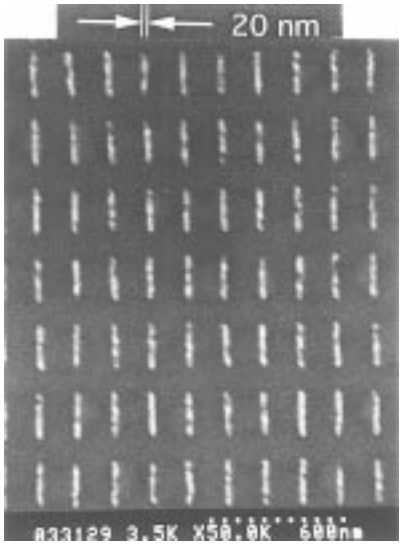

Fig. 3. SEM image of an interactive Ni bar array. Each bar is 20-nm wide, 200-nm long, and 35-nm thick.

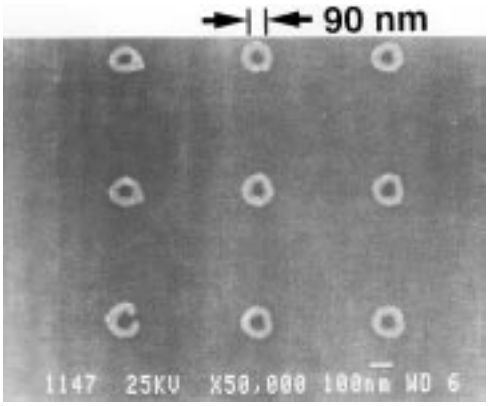

Fig. 4. SEM image of Ni rings of a 90-nm mean diameter, 25-nm ring width, and 35-nm thick on Si.

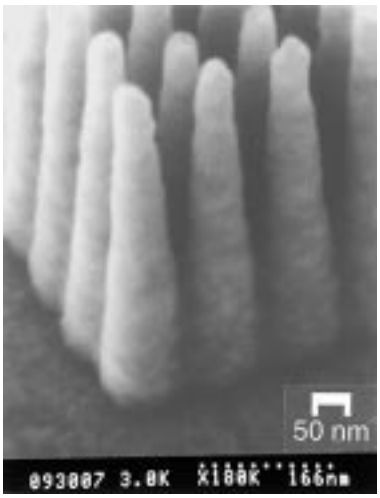

Fig. 5. SEM image of Ni pillar array of a 75-nm average diameter, 700-nm height, and 100-nm spacing fabricated using e-beam lithography and plating.

be overcome to make development of PMN attractive. In 1995, the NanoStructure Laboratory proposed and

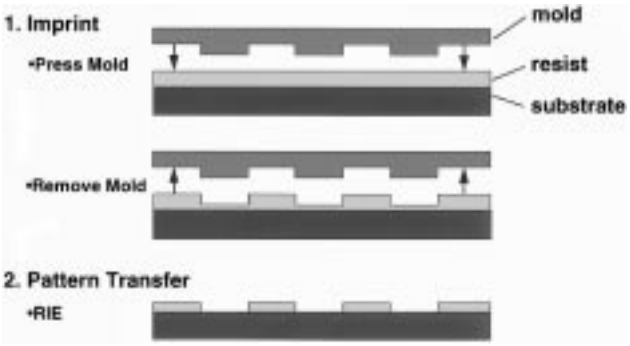

Fig. 6. Schematic of nanoimprint lithography, consisting of 1) imprint and 2) pattern transfer.

demonstrated nanoimprint lithography—a new lithographic paradigm that offers ultra-high-resolution, high-throughput, low-cost manufacturing of nanostructures [18], [19]. Nanoimprint lithography is opening the door for commercialization of many innovative nanodevices and makes development of patterned magnetic nanostructures very attractive.

Nanoimprint lithography has two steps (Fig. 6). The first is imprinting in which a mold with nanoscale features is pressed into a thin resist cast on a substrate, creating a thickness contrast pattern in the resist. The second step is pattern transfer. After removing the mold, an anisotropic etching is used to transfer the pattern into the entire resist thickness by removing the remaining resist in the compressed areas. In one of the imprint methods, the resist is a thermoplastic polymer which is heated during the imprint to soften the polymer relative to the mold. If the temperature is above the polymer's glass-transition temperature, the polymer becomes a viscous liquid and can flow, and thereby can be readily deformed to the shape of the mold. The mold can be made of metals, dielectrics, or semiconductors. Very recently, we achieved 10-nm features with 40-nm period corresponding to 400 Gdots/in^2 (Fig. 7).

V. Size and Shape Effects on Properties of Patterned Magnetic Nanostructures

A. Background

In the demagnetized state, a thin-film or a bulk magnetic material is magnetically divided into many small regions, called "domains." Each domain, typically containing a number of polycrystalline grains, is spontaneously magnetized, but with a random magnetization direction, so that the material as whole has no magnetization and the total energy is minimized (which is the sum of magnetostatic energy, exchange energy, crystalline anisotropy energy, magnetorestriction energy, and Zeeman energy) [25]. Since there are many local energy minimum with each of them corresponding to a number of magnetic configurations, the exact magnetic domain configuration in a thin film or bulk material is rather unpredictable.

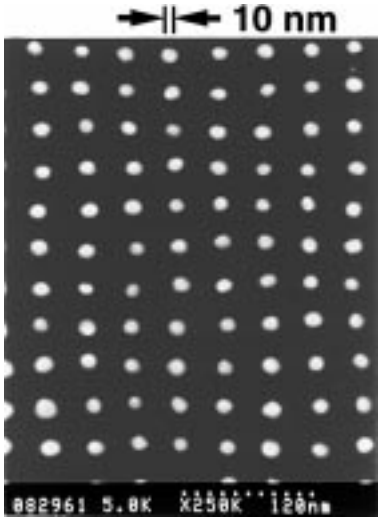

Fig. 7. SEM image of 10-nm-diameter Ti/Au dots with 40-nm pitch fabricated using nanoimprint lithography and lift-off.

Things are drastically different, however, when a magnetic material is patterned into a size comparable to a single domain size [25]. In this case, each PMN contains only one or a few domains; the size, shape, and orientation of each domain become *well defined and predictable*. The unique features of a PMN are attributed to new interplay between the magnetostatic energy and exchange energy. The discontinuity of magnetization at the edges of a PMN can create magnetic poles, thereby, increasing the magnetostatic energy. As sample size becomes comparable to the domain wall size, formation of multidomain becomes difficult. All these lead to a new balance of the energy equation.

B. Spontaneous Formation of Single Domain

The first important property of a patterned magnetic nanostructure is that a single domain can be formed spontaneously without an applied magnetic field. Namely, the structure becomes a magnetic dipole on its own as soon as it is fabricated. This is a consequence of interplay between the magnetostatic energy and exchange energy. To reduce the exchange energy, it favors the alignment of all magnetic domains in the same direction (i.e., ferromagnetism), forming a single domain. On the other hand, to reduce the magnetostatic energy, it favors breaking the material into multiple domains to cancel out magnetic poles. A simple estimate indicates that the magnetostatic energy for a single-domain cube of a side of L is proportional to its volume (L^3). For a multidomain cube of a side L, the domain wall energy is proportional to area (L^2), hence the total energy of a multiple domain cube (sum of the magnetostatic and exchange energy) is approximately proportional to $L^{2.5}$ [25]. Therefore, there is a critical size below which the single-domain state has the lowest energy, but above which the multiple domain state has the lowest energy. This critical size, determined by the magnetization and exchange constant of a material, is about 100–300 nm in a thin film.

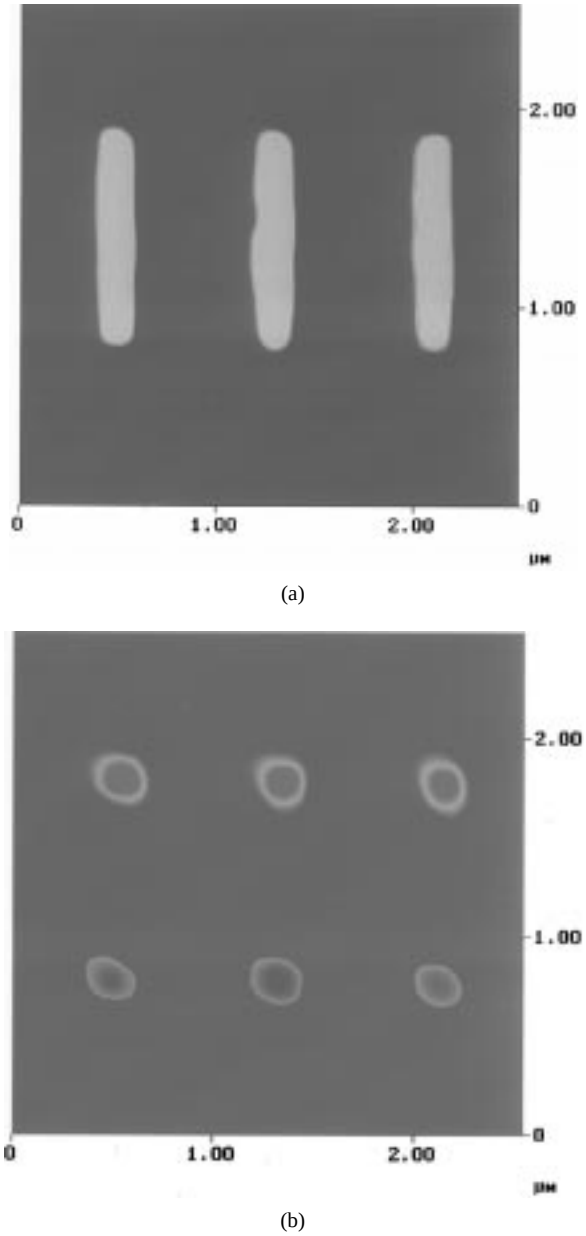

Fig. 8. (a) The atomic force microscopy and (b) magnetic force microscopy of three single-domain nickel bars that are 100-nm wide, 1-μm long, and 35-nm thick. The red represents attractive force between the tip and the sample and the blue repulsive force.

C. Control of Domain Configurations Using Shape

The magnetization direction in a single domain and multidomain PMN can be well controlled by the shape of the structure. In a single domain, the stable magnetization is always along the long axis of the structure, to reduce demagnetization field and lower the total energy. Fig. 8 shows both AFM and MFM images of Ni bars which are 1-μm long, 100-nm wide, and 35-nm thick. The MFM image exhibits only two opposite magnetic poles at the two ends of the bars—characteristic of a single magnetic domain.

In a multi-domain PMN, the magnetization at the edges tends to be parallel to the edge to avoid free magnetic poles for lowering the magnetostatic energy (the surface pole

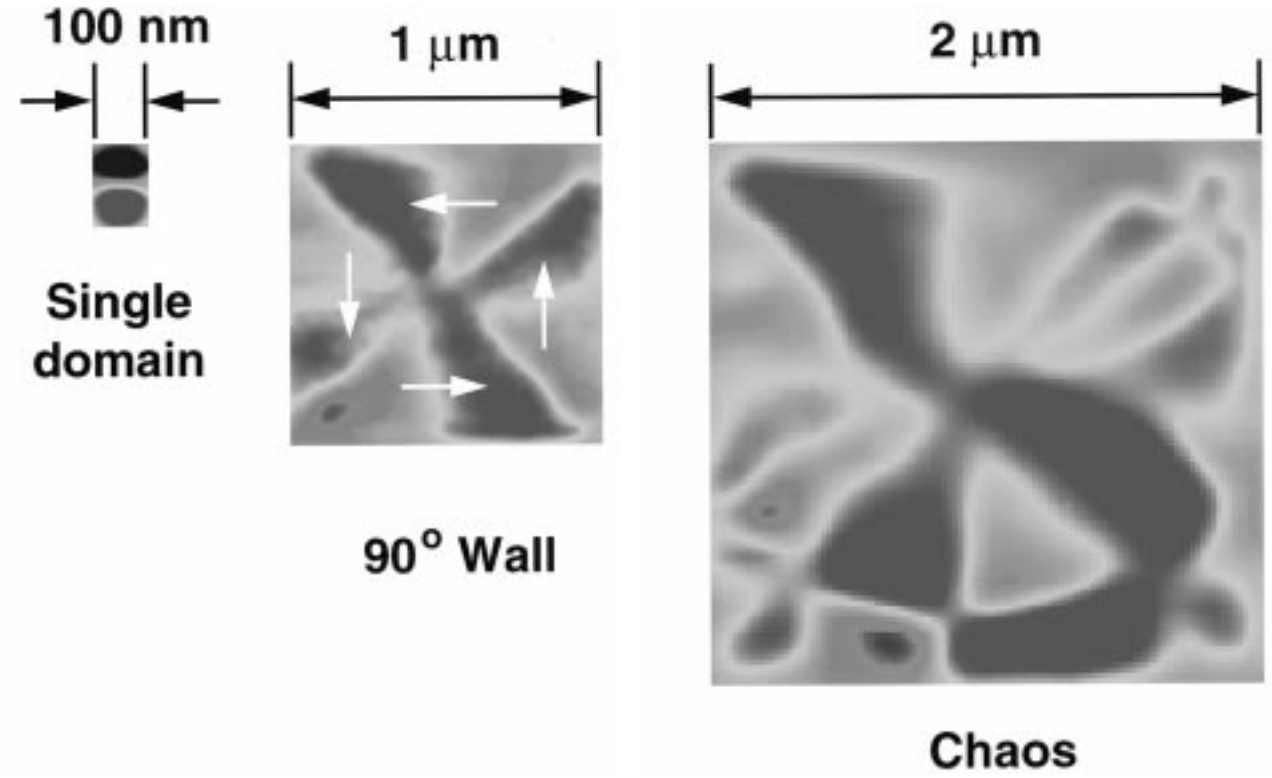

Fig. 9. MFM images of magnetic domains in cobalt squares (35 nm thick) as their sizes are reduced from 2 μm to 100 nm. The red represents attractive force between MFM tip and sample and the blue repulsive force.

density is equal to the discontinuity of the magnetization normal to the surface). Fig. 9 shows the MFM images of magnetic domains in cobalt squares (35-nm thick) as their sizes are reduced from 2 to 100 μm. At 2 μm, the domain configuration is chaos. At 1 μm, it has four well-defined closure domains. At 100 nm, it is a single domain.

Ni rings were also studied. No magnetic flux was detected by MFM, indicating all flux is confined inside the rings. Currently, a scanning electron microscopy with polarization analyzer (SEMPA) is used to observe the confined flux.

D. Effects of Bar Width on Switching Field

Another key property of PMN is that the coercivity—the magnetic field needed to switch the magnetization direction—can be controlled by changing the structure's size and shape anisotropy. This is again a consequence of the interplay between the magnetostatic energy and exchange energy.

To investigate this property in PMN, we fabricated nickel and cobalt bars of 35-nm thickness and different width and shape anisotropies using e-beam lithography, thermal evaporation, and lift-off. Thermal evaporation, instead of sputtering, eliminates crystalline anisotropy in the materials that could mask the shape anisotropy effect. Vibrating sample magnetometer measurements show that the unpatterned thin-film samples, fabricated together with the bar samples, have a coercivity of 50 Oe for Co and 25 Oe for Ni, and have near zero crystalline anisotropy.

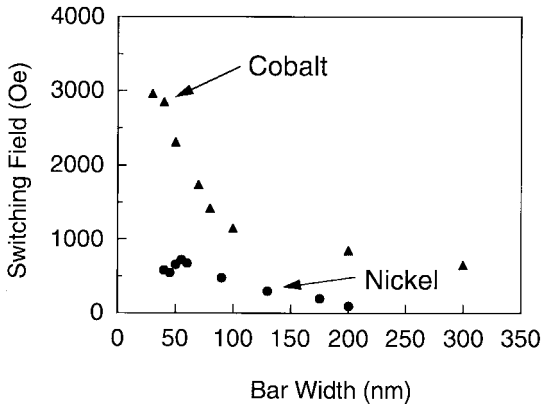

Fig. 10. Switching field of isolated Ni and Co bars versus bar width. The bar width was measured using SEM. The bars are 1-μm long and 35-nm thick.

The switching fields of isolated Co and Ni bars with a 1-μm length and 35-nm thickness as a function of the bar width were measured by using an external field and MFM and are shown in Fig. 10 [16], [26]. For Co bars, the switching field increases monotonically with reduction of the bar width, reaching 3000 Oe at 30-nm width. The switching field is 60 times higher than that of the unpatterned thin film. For the Ni bars, the switching field first increases with decreasing bar width, reaches a maximum switching field of 740 Oe (30 times higher than that of the thin film) at a bar width of 55 nm, then decreases slightly with further reduction of the bar width. The decrease is likely

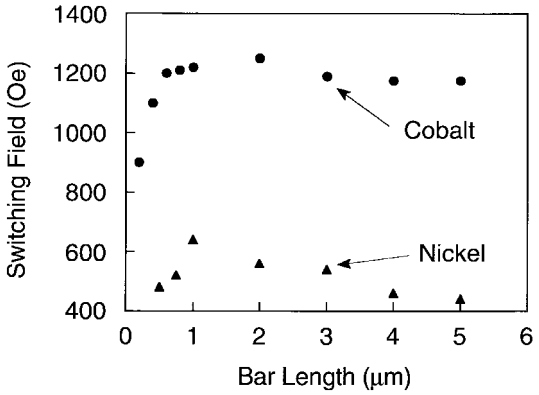

Fig. 11. Switching field of isolated Ni and Co bars versus bar length. The bars are 100-nm wide and 35-nm thick.

due to the fact that thermal energy becomes comparable to magnetization switching energy [25]. The Ni bar width dependence is similar to Permalloy bar studied by the UCSD group [27]. Furthermore, the MFM shows that for 1-μm bar length and 35-nm thickness, the critical width to form single domain is 300 nm for Co and 150 nm for Ni, respectively.

E. Effects of Bar Length on Switching Field

The effects of bar length on Co and Ni bars with a fixed bar width and thickness (100 and 35 nm, respectively) were also investigated. Unlike the bar width dependence, the switching field of the single-domain bars was found to first increase with the bar length, then decrease after reaching a peak (Fig. 11). The peak switching field and the corresponding bar length are 640 Oe and 1 μm for Ni, and 1250 Oe and 2 μm for Co, respectively. Furthermore, the switching field of Ni bars decreases with the increase of the bar width much faster than that in Co bars. The length dependence observed here does not fit the Stoner–Wohlfarth model, which predicts a *coherent* switching, meaning the switching field of a bar should monotonically increase with the shape anisotropy (therefore with the bar length) [28].

The nonmonotonic length dependence suggests that different bar lengths have different switching mechanisms. For short bars (<1 μm) where the bar length is comparable to domain wall size, all spins would rotate more or less in a same fashion, leading to a quasicoherent switching. For long bars where the bar length is significantly longer than the domain wall, the exchange force is not strong enough to keep all spins rotating in the same way. In this case, the domain reversal occurs at the ends of the bar where demagnetization field is the strongest, and the reversal propagates through the entire bar, leading to an incoherent switching. As Co has much stronger exchange force than that in Ni, Co bars should have a longer crossover length than that in Ni, consistent with experimental results.

Although the switching speed of PMN has not been measured yet, it is expected that coherent switching has

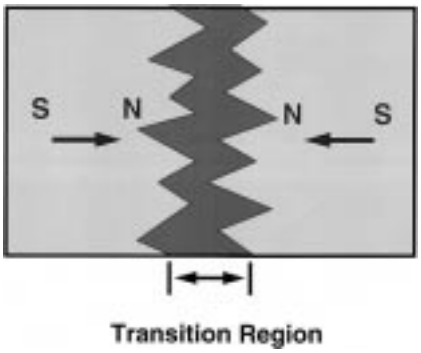

Fig. 12. Schematic of transition region between two bits for the conventional magnetic recording media.

time scale of 1 ns, and incoherent switching should be the bar length divided by the domain propagation speed.

VI. Quantized Magnetic Disks

As we enter the information epic, demands for higher data storage density in magnetic memories escalate drastically. Since 1990, the area data storage density of hard disk drives is increasing at a rate of 60% a year, already reaching 1 Gb/in^2 for commercial products and 5 Gb/in^2 for experimental disks [29]. Following the 60% growth rate, the storage density of commercial disks should reach 10 Gb/in^2 in the year of 2001 [30]–[34]. Whether such density is achievable is still under debate. One thought is that for a storage density significantly higher than 10 Gb/in^2, a new magnetic disk paradigm is needed.

The ultimate storage density of a magnetic disk is related to magnetic recording media, write head, read head, position and servo, and signal processing. Although they are intricately related, the most important of all is the media which dictates the requirement to all others. A good media will relax the requirements. Following discussion focuses on a new medium.

A. Factors Limiting Storage Density in Conventional Magnetic Media

The present magnetic media is a continuous, thin, magnetic film supported by a rigid, nonmagnetic disk. The film consists of many tiny, polycrystalline grains with a rather broad distribution in size and shape and a random distribution of crystallization direction. The magnetization orientation of these grains is also random until a magnetic field created by a write head aligns the magnetization of a tiny patch of these grains. The data is represented by the magnetic moment, area, size, and location of this patch.

Four factors limit the storage density capacity in a thin-film media. The first is the "superparamagnetic limit." Because of the statistical nature in the size and easy-magnetization axis of polycrystalline grains in a magnetic media, the intrinsic signal-to-noise ratio (SNR) of a magnetic signal roughly equals the number of grains in each bit.

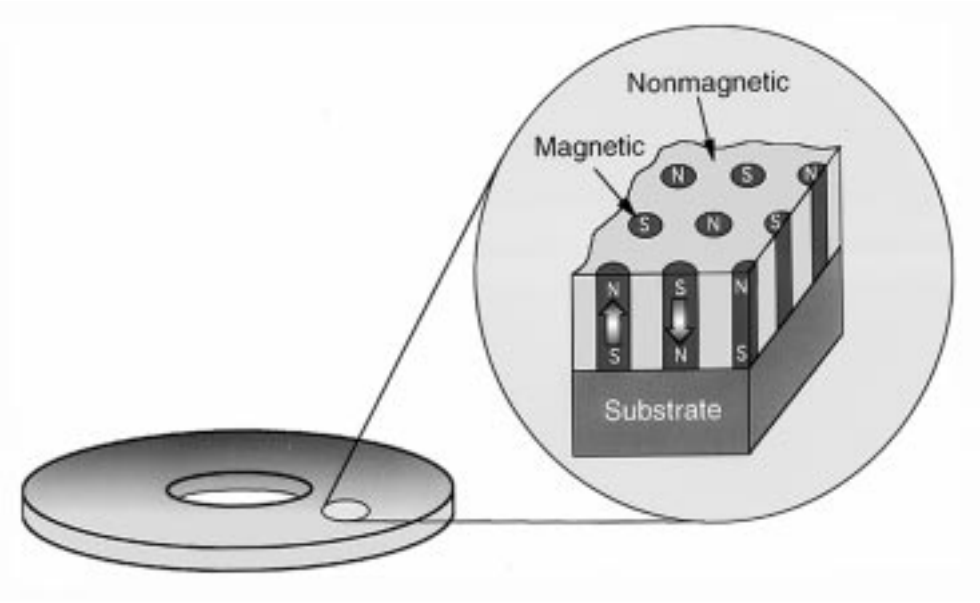

Fig. 13. Schematic of a quantized magnetic disk which consists of patterned, single-domain, magnetic structures uniformly embedded in a nonmagnetic disk.

To reduce bit size while keeping the same SNR requires a reduction of the grain size. But, when each grain becomes too small and weakly coupled to its neighboring grains by the exchange force, the energy needed to switch the magnetization of a grain can becomes less than the thermal energy. Should that happen, thermal energy will wipe out the written data. For an isolated magnetic sphere, the superparamagnetic limit will be reached when the diameter is below 9 nm. To maintain the well accepted SNR, namely 1000 grains, the superparamagnetic limit gives a maximum data density of 8 Gb/in^2, insufficient to meet our needs [30].

The second limiting factor is the transition width between two neighboring bits of opposite magnetization. The nature of ferromagnetism, namely the positive exchange integral, (which occurs only in a few elements such as Co, Ni, and Fe) favors all magnetization aligned in the same direction. When one bit is placed next to another bit with an opposite magnetization, a transition region, called a domain wall, must be formed for reducing exchange energy. Certainly, the spacing between two bits cannot be smaller than the domain wall size. Furthermore, to lower the total energy, the interplay between the magnetostatic force and the exchange force makes the transition region between two bits have a random zig-zag shape (so-called Neel spikes), as shown in Fig. 12. The zig-zags would not only increase the effective width of a transition region, but also create noise in the reading signal (since the reading head, having a straight line shape, averages the positive and negative magnetic charges in the zig-zags). The effective transition region for today's conventional medium is 40–80 nm.

The third factor is the "side tracks." The magnetic field distribution of a write head is not perfect; the fringing field at the sides of a tip pole in a write head writes two tracks of junk next to the data (called "sidetracks"). Since the sidetracks erase previously written data, extra space between two data tracks must be reserved for the side tracks, limiting data packing density.

The fourth factor is the "tracking." Conventional magnetic medium does not automatically provide a tracking signal since a physical boundary does not always exist between two neighboring bits (it exists only between two bits of opposite magnetization). Hence, writing or reading a bit is a "blind" process. The head first locates special codes (tacking marks) written at the beginning part of each data section, then calculates the movement between the head and the disk to get the "supposed" bit location. Therefore, the accuracy of the disk rotation and servo will impose another limit of data density. Furthermore, much real estate area and time are wasted in writing the tracking marks, which currently use about 20% of the total disk area and should use more area for higher data density where tracking is more crucial.

B. Concept of Quantized Magnetic Disks

All of the limitations listed in the last section can be removed or alleviated if the continuous, thin-film media is replaced by a new media, quantized magnetic disks (QMD's). QMD's have discrete, single-domain magnetic elements uniformly embedded in a nonmagnetic disk (Fig. 13) [15]. Each single-domain element has a uniform, well-defined shape, a prespecified location, and most importantly, a discrete magnetization that is magnetized without an applied magnetic field and has only two possible stable states: equal in magnitude but opposite in direction. The spontaneous formation of a single domain is due to its small size and shape anisotropy (as discussed in Section V-B). Each magnetization direction of a single-domain element represents a bit of binary information. A QMD

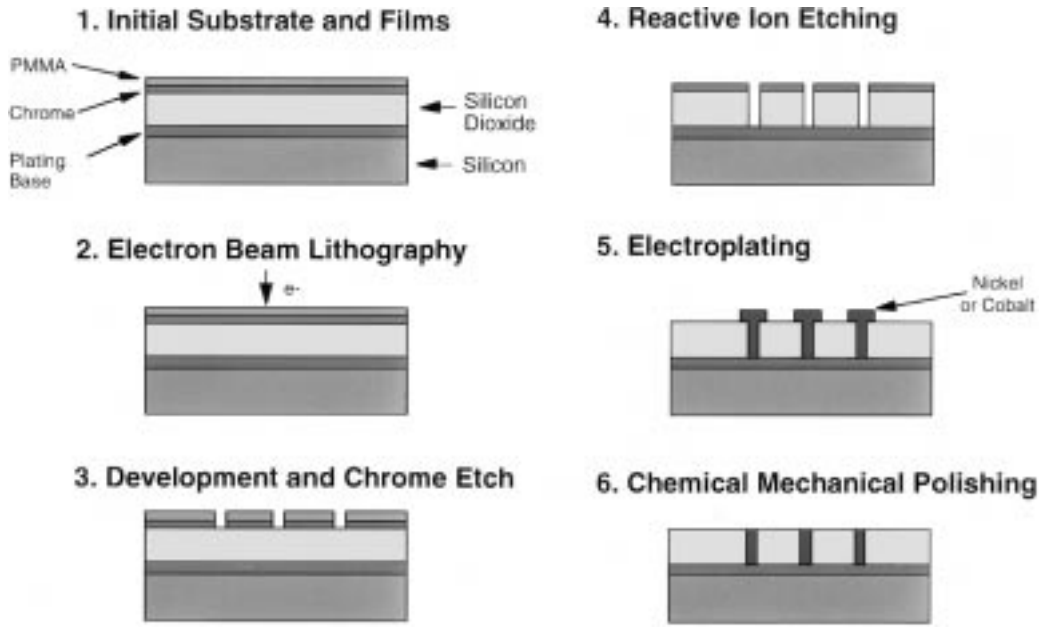

Fig. 14. Schematic of vertical QMD fabrication process.

of a vertical magnetization uses pillars (Fig. 13) and a longitudinal magnetization uses bars (Fig. 2). The magnetic field needed to switch the magnetization direction can be controlled by engineering the element's size and shape anisotropy (discussed in Sections V-D and V-E) [16].

QMD's have many advantages over the conventional disks such as spontaneous self-quantization of each bit's magnetization; quantized writing process to reduce requirements on write head and position accuracy; small, smooth, isolated transition region allowing high data-packing density and near-zero transition noise; built-in tracking making for precision tracking and position of write/read heads; and overcome of the superparamagnetic limits.

The idea of storing one bit of information in a tiny single-domain magnetic particle could have been speculated when single-domain structure was observed [35] or when single-domain particles were used in making recording tapes. The theory of coherent switching of a single-domain particle has been discussed in the celebrated paper by Stoner and Wohlfarth (note the switching of the patterned single-domain element is usually incoherent). Many other behaviors of single-domain structures were theoretically investigated by Aharoni [36]–[38]. A number of unique properties of single-domain element as a storage element in QMD's, however, were not explored until four years ago when two advanced technologies became available. One is the nanofabrication technology that enables us to precisely engineer the shape, size, location, orientation, and composition of a single-domain magnetic particle [14], [16], [39], [40]. The other is magnetic force microscope that allows us to image and manipulate the magnetic properties of each individual single-domain particle. Recently, the advent of imprint lithography brightens the commercial aspects of QMD's.

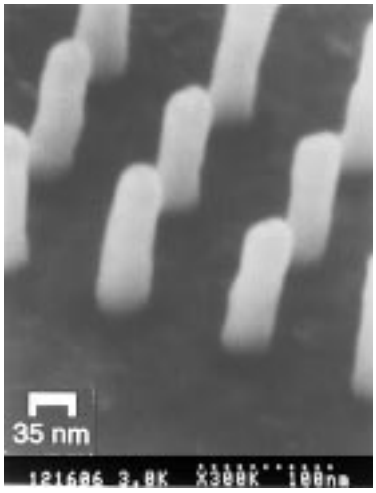

Fig. 15. SEM image of Ni pillar array of 35-nm diameter, 120-nm height, and 100-nm spacing. The density is 65 Gb/in^2 and the aspect ratio is 3.4.

A number of names have been given to QMD. Each of them emphasizes a part of the disk's characteristics. QMD stresses the quantized nature of the magnetization, location, writing, and tracking of each bit. "Patterned magnetic disk" (PMD) stresses the method of fabricating the disk. "Discrete magnetic disk" (DMD) seems to be a combination of QMD and PMD, but could be confused with "discrete track disk" [41], [42] and "discrete segment disk" [43], [44], which have been studied prior to QMD's and are fundamentally different from QMD's. Another possible choice is "patterned single-domain magnetic disk" (PSMD).

C. Structure and Fabrication of 65-Gb/in^2 Vertical QMD's

Various structures and fabrication methods for longitudinal and vertical QMD's have been developed [45]. Vertical QMD's are discussed in this section and longitu-

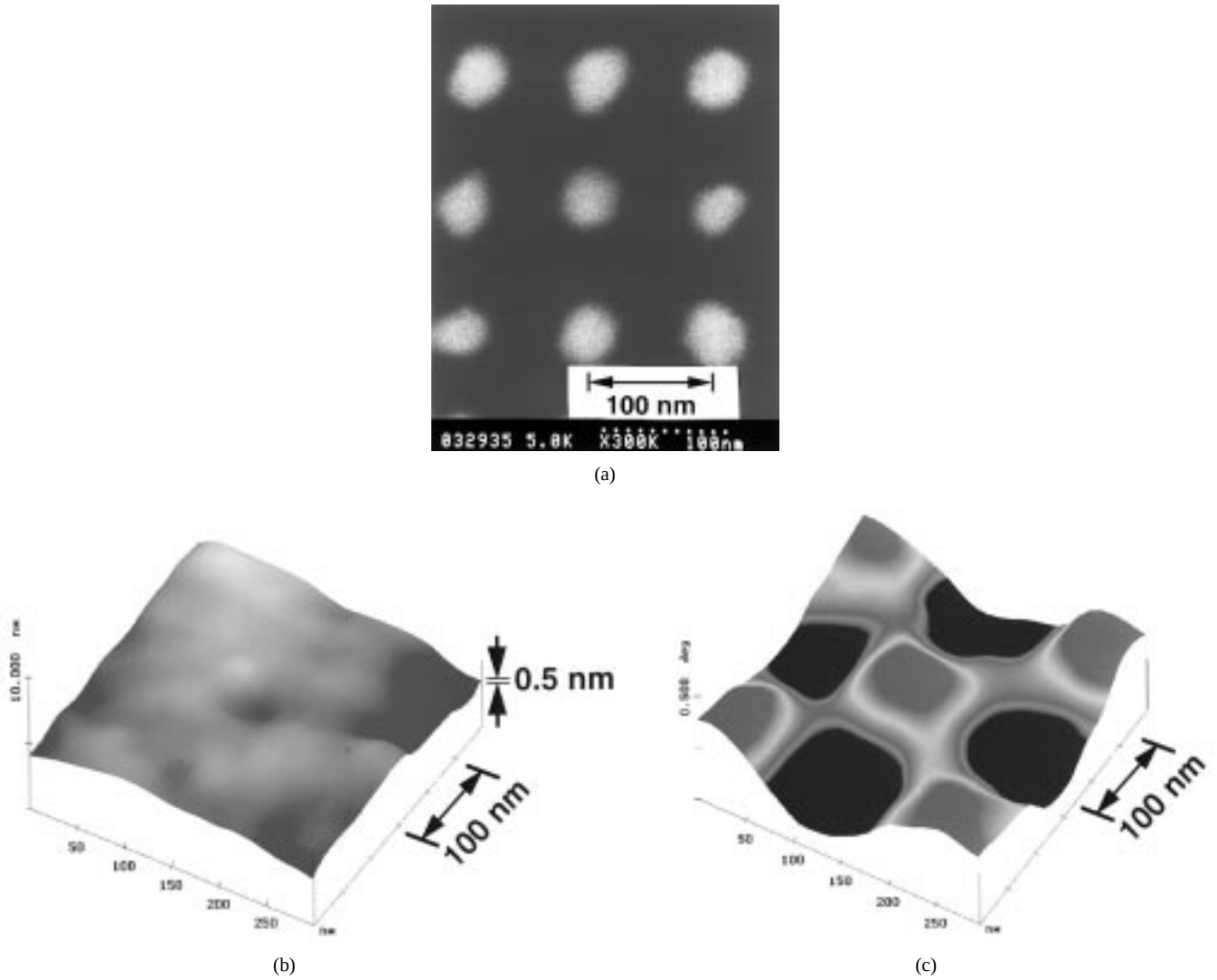

(a)

(b)

(c)

Fig. 16. (a) SEM image, (b) TMAFM image, and (c) MFM image of 3 × 3 b of a QMD with 65-Gb/in^2 density. The red represents attractive force between tip and sample and the blue repulsive force. Each bit consists of a nickel pillar uniformly embedded in 200-nm SiO_2 with a 50-nm diameter (aspect ratio of 4) and a 100-nm period. The TMAFM image shows a very smooth surface with a roughness of 0.5-nm RMS. The MFM image shows an alternating pattern of magnetization directions from each bit.

dinal QMD's in the next section. One of the vertical QMD structures consists of ultra-high-density arrays of nanoscale single-domain nickel pillars embedded in a SiO_2 film with an extremely smooth top surface [46]. The fabrication begins by depositing on a silicon substrate a thin metal plating base, SiO_2 film, chrome film, and PMMA film (Fig. 14). First, electron beam lithography was used to expose dot arrays in the PMMA. After developing, the dot arrays were transferred into the holes in chrome film by wet etching. Second, reactive ion etching was used to etch the array of holes in SiO_2 to expose the plating base. Third, an electroplating process was used to selectively plate nickel into the SiO_2 template openings. Fourth, chemical mechanical polishing was used to remove overplated nickel giving a very smooth surface. The sidewall of the pillars is straight, as shown by the SEM image in Fig. 15, where the oxide is removed. To save e-beam exposure time, only a section of QMD was fabricated.

The properties of the QMD have been investigated using scanning electron microscopy (SEM), tapping mode atomic force microscopy (TMAFM), and magnetic force microscopy (MFM) [45]. An SEM micrograph of a 3-b by 3-b section of the QMD in a top view is shown in Fig. 16(a). The micrograph shows that the nickel pillars of the QMD have a 50-nm diameter and a 100-nm period. The pillars are 200-nm tall and thus have an aspect ratio of four.

TMAFM and MFM images taken simultaneously on the same area of the QMD are shown in Fig. 16(b) and (c), respectively. The TMAFM image of a 3 × 3-b section of the QMD shows that the topology of the nickel pillars is indistinguishable from that of the SiO_2. The surface has a root-mean-squared roughness of 0.5 nm. The corresponding MFM image, on the other hand, clearly shows that each bit has a quantized magnetization orientation and the magnetic image of each pillar of the 9-b section can be resolved.

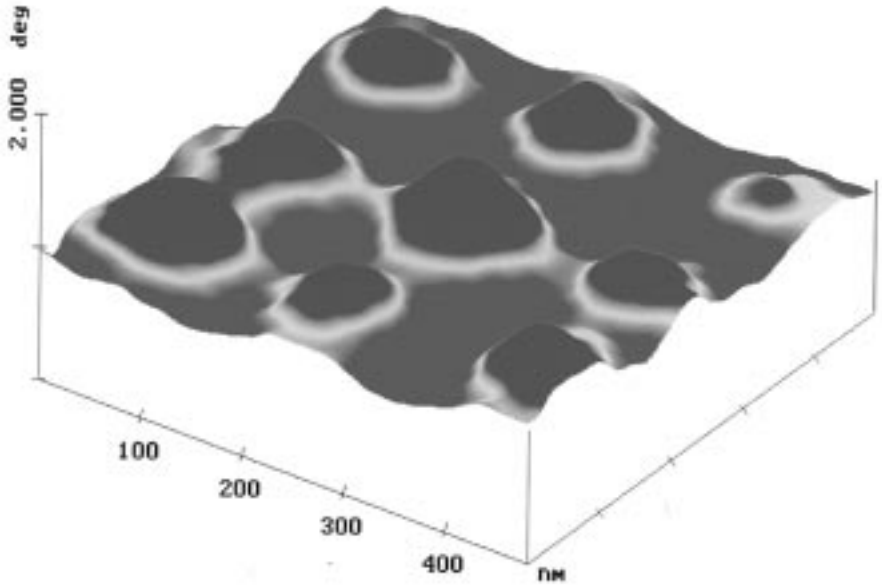

Fig. 17. MFM images of 3 × 3 bits of a vertical QMD that have the same magnetization direction.

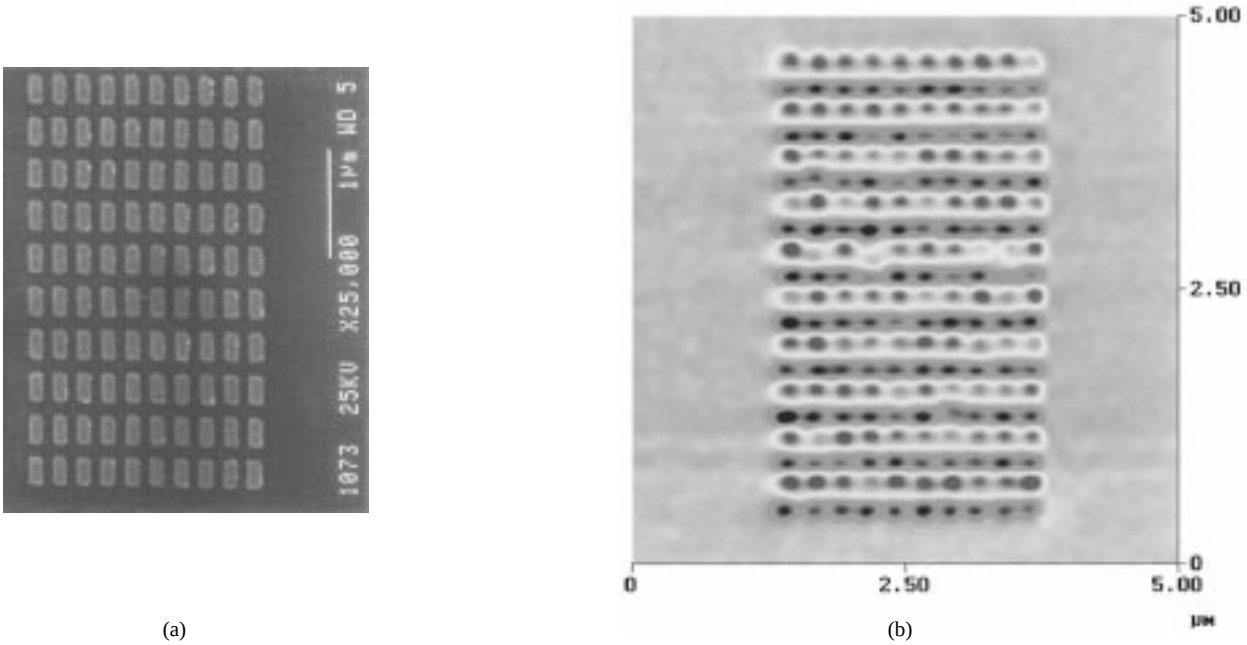

(a) (b)

Fig. 18. (a) SEM and (b) MFM images of discrete single domain Co bars with a 70-nm width, 240-nm length, and 150-nm spacing on silicon, which corresponds to a 7.5-Gb/in^2 density. The red represents attractive force between tip and sample and the blue repulsive force.

Five bits have the south pole (red) on the top surface and the other four bits have the north pole (blue) on the top. The QMD was demagnetized before imaging, therefore the nearest neighbor bits have opposite magnetization directions. This magnetization configuration is the lowest energy state for the QMD. Furthermore, the MFM images of nine bits of the same magnetization direction are shown in Fig. 17. Our study also showed that the nickel pillar can be switched using a MFM tip with a large magnetic moment. The storage density of the QMD section is 65 Gb/in^2, which is over two orders of magnitude higher than that of state-of-the-art commercial magnetic disks.

D. Structure and Fabrication of 7.5-Gb/in^2 Longitudinal QMD's

Longitudinal QMD's were fabricated as well [47]. One of the advantages of longitudinal QMD's over vertical QMD's is that writing a longitudinal QMD with a MFM tip does not require changing of the magnetization direction of the MFM tip. A simple way to fabricate longitudinal QMD's is by lift-off of Ni or Co bars on a substrate. Fig. 18 shows images of discrete single domain Co bars with a 70-nm width, 250-nm length, and 150-nm spacing on silicon, which corresponds to a 7.5-Gb/in^2 density fabricated using

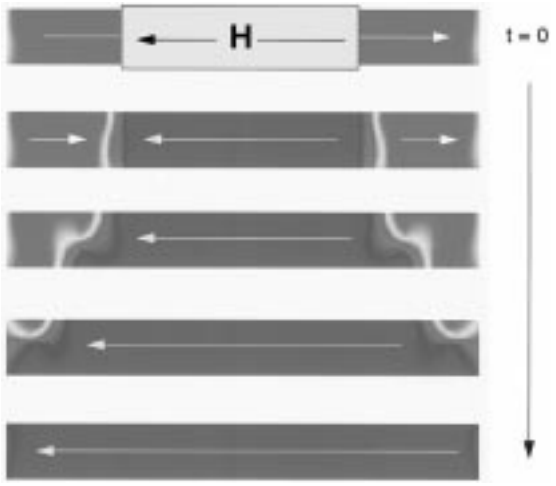

Fig. 19. A writing process where the writing field with a size only half of the bar length was located in the middle of the single-domain bar.

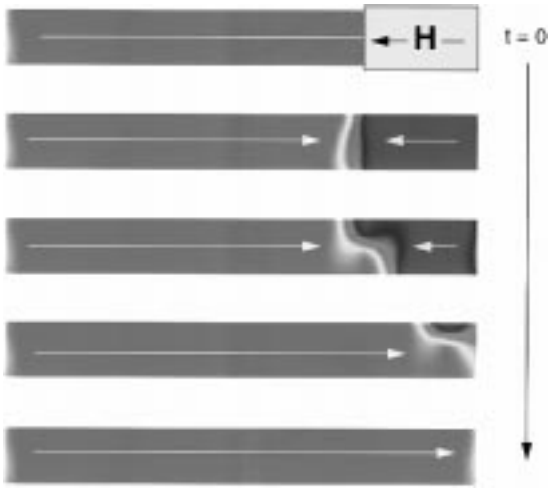

Fig. 20. A writing process where the writing field overlaps only one quarter of the bar length.

nanoimprint lithography. Such disks have the gaps between the bits, but if the gap is small compared with the head slide, the gap may not damage the head. For a smooth surface, similar fabrication approach discussed in last section can be used.

E. Discrete Magnetization and Quantized Writing Process

Since each bit in a QMD spontaneously magnetizes itself without an applied field and has only two opposite stable magnetization states, the write process in a QMD is quantized with three unique features. First, in contrast to conventional disks where the magnetic moments, area, and location of each bit must be precisely defined by a write head, in QMD's they are already defined when the disk was fabricated. Thus, the writing process in a QMD is a simple flip of the magnetic direction of a discrete single-domain bit. A write head either writes the entire bit perfectly or it does not write the bit at all. Second, each bit in QMD can be written perfectly with a write field smaller than the size of the bit [48]. Third, a minor overlap of the writing field with a nearby bit perturbs only temporarily the magnetic moment of the bit. Once the overlapping writing field is removed, the bit returns to its original magnetic state. Clearly, the quantized writing in a QMD greatly relaxes the requirements on the write head design and position accuracy, and significantly avoids the writing errors and side-tracks. All of these advantages lead to a higher data storage density.

Now let us look at the quantized writing process using micromagnetic simulation and MFM measurement [48]. The simulation finds the equilibrium magnetization configuration of a ferromagnetic body by minimizing its total energy (a sum of magnetostatic energy, exchange energy, crystalline anisotropy energy, and Zeeman energy) [49]–[56]. It is assumed that a bit in a QMD is a polycrystalline cobalt bar of 35-nm thickness, 100-nm width, and 1-μm length with a coercivity of 1100 Oe [26], a saturation magnetization of 1422 emu/cm^3 [25], and the exchange constant of 6.0×10^{-6} erg/cm. The write field was assumed to be uniform, twice the coercivity, and in the opposite direction to the initial magnetic moment of the bit. Simulation showed that if the writing field covers over 50% of the area of the single-domain bit, the bit will be written perfectly; but if it covers less than 50%, the bit will preserve its original magnetic state. Two examples are given below [48].

Fig. 19 shows that the overlap is only 50%. The switching occurred roughly in two stages. Initially, the magnetic moments in the region under the writing field were reversed. Then, due to the exchange force and shape anisotropy, the reversal propagated out of the write field region and reached the entire bit. Fig. 20 shows the case where a writing field covers only one quarter of the bar length. The writing field reverses only the magnetic moment in the overlapped region, but no further propagation occurred because the shape anisotropy of the section outside of the field is greater. Once the writing field was removed from the bar, due to the exchange force, the section with a large shape anisotropy will drive the magnetic moment of the entire bar back to its original state.

The quantized writing process in a QMD is analogous to moving a ball between two valleys separated by a mountain (each valley represents one of the two energy minimums). Once the ball is pushed from one valley over the top of the mountain, it will roll down to the other valley on its own (perfect writing). But, if the ball is released before being pushed over the top, it will go back its original valley (no writing) (Fig. 21).

The quantized writing process has been confirmed experimentally using a MFM tip [47]. The magnetic field of a MFM tip splits, at the tip point, into two halves: one pointing in one direction and another in opposite direction. As the tip is moving from one end of a single-domain bar to the other end, the overlap between the bar and the field in the moving direction decreases and the overlap between the bar and the field in the opposite direction increases (Fig. 22). If the bar can be switched using a magnetic field of a size smaller than that of the bar, then the magnetization direction of the single-domain bar will be changed before

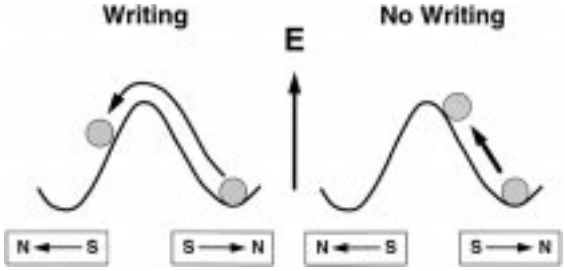

(a) (b)

Fig. 21. Schematic illustrating that the quantized switching process of a single-domain structure is like moving a ball over a hill. (a) The ball, once over a hill, will roll to another state itself and (b) once the drive force is removed, the ball, before reaching the top of the hill, will roll back to the original state.

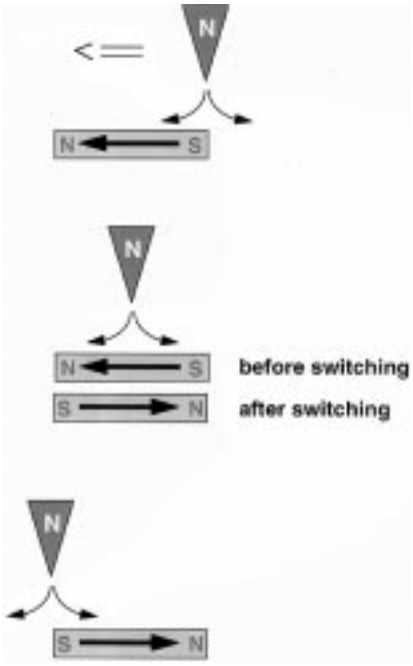

Fig. 22. Schematic of the QMD writing process using a MFM tip.

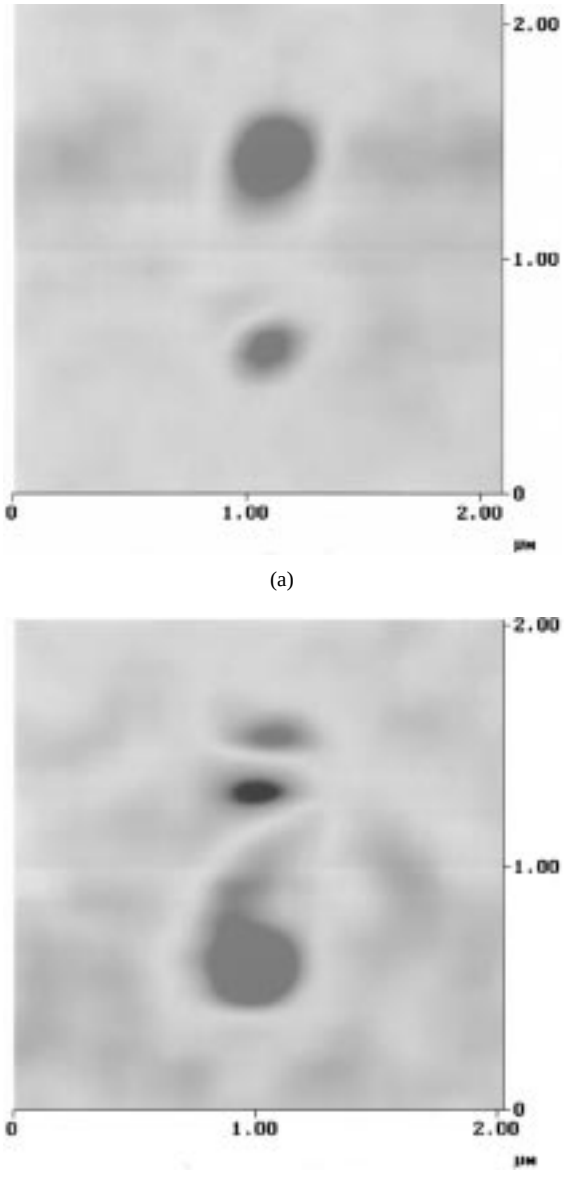

Fig. 23. (a) MFM image where the poles at the two ends of the bar have identical polarization, confirming that the magnetization of the single-domain bar is switched by the MFM tip having a field of a size smaller than that of the bar. (b) MFM image where the switching occurred when a MFM tip is near the end of the scan, the MFM image has a perfect north pole at the starting end of the bar, but, at the finishing end, only half of a south pole (before the switching) and half of a north pole (after the switching).

the MFM tip reaches the other end of the bar. In this case, the magnetic images of the bar will display two poles with the identical magnetic polarization (e.g., two south poles). This is because for a single-domain bar, no magnetic charge can be seen anywhere except at the two ends of the bar. At the end where scanning starts, the MFM sees one pole before the bar is switched and at the finishing end, the MFM sees another pole after being switched. Since the magnetization switches much faster than the MFM scanning speed, the MFM image cannot tell the occurrence of the switch until the tip reaches the other end.

Magnetic image of a single domain bar in Fig. 23(a) shows that the poles at the two ends of the bar indeed have the identical polarization, confirming that the magnetization of the single-domain bar is switched by the MFM tip with a field size smaller than that of the bar.

When using a weaker switching field, a larger overlap between the switching field and the bar is required. Fig. 23(b) shows that switching occurred when a MFM tip is near the end of a scan, therefore the MFM image having a perfect north pole at the starting end of the bar, but, at the finishing end it had only half of a south pole (before the switching) and half of a north pole (after the switching). The weaker switching field can be achieved by either reducing the amount magnetic material on a MFM tip during the tip fabrication or increasing the spacing between the MFM tip and the bar.

Writing of a 7.5-Gb/in^2 longitudinal QMD using a MFM tip is shown in Fig. 24(a) and (b) [47]. Clearly the writing process is quantized and perfect. The writing experiment

was done using two MFM tips: the writing tip with a large magnetic moment and the reading tip with very small magnetic moment (so that it would not flip the magnetization of the bar). Before writing, the magnetization of all the bars were aligned in the same direction. During the writing process, the writing tip was lifted up and then was moved to one end of a bar. The end of the bar initially had a magnetic pole opposite to that of the MFM writing tip. The actual writing process was simply to lower the writing tip, making the tip closer to the bar. It was found that when the separation between the tip and bar was less than 5 nm, the writing tip could perfectly flip the magnetization direction of the bar *without* flipping the neighboring bars, even at a data density of 7.5 Gb/in^2. After writing one bar, the MFM writing tip was raised up and moved to write other bars. This process was continued until all the desired bars were written. After writing, the reading tip was used to nondestructively image the written pattern.

It should be pointed out that the MFM tip does not have a well-defined field distribution, and that the MFM does not have any feedback to track the exact tip movement leading to a poor positioning accuracy (about 1% of the scanning window size). Also, the switching field of each bar is not exactly the same due to the fabrication imperfection and magnetostatic interaction between the bars. However, even under these circumstances, the 7.5-Gb/in^2 longitudinal QMD can be written perfectly. This clearly demonstrates the advantage of quantized writing process of QMD in ultra-high-density recording. Namely, quantized nature of the QMD relaxes the requirement of the writing field and can increase the tolerance toward the errors due to head positioning and fringing field.

F. Cut-Off Interbit Exchange Force, Small, and Smooth Transition, Less Noise

Since the exchange force has an effective range less than 10 nm, a thin layer of nonmagnetic material between two neighboring bits in a QMD can completely cut off the exchange force between the bits, leading a "transition region" that is much smaller than the transition region in a thin film magnetic media, where each grain is more or less coupled by exchange force. Furthermore, the nonmagnetic materials, patterned by a nanofabrication technique, can have very smooth and straight edges, giving a much quieter reading signal than that in a thin-film media where the transition regions have a zig-zag shape.

G. Built-In Tracking Marks, Precise Tracking

In a QMD, since each discrete bit is a single domain, isolated by nonmagnetic materials, and spontaneously magnetized, a variation in the magnetic field always exists between neighboring bits, regardless of the polarization of each bit. This provides a signal for tracking each bit. In other words, in a QMD drive, discrete single-domain elements automatically provide a "landmark;" each bit can be physically "seen" prior to writing or reading, allowing much more precise tracking than the "blind tracking" in a conventional disk and therefore higher data density.

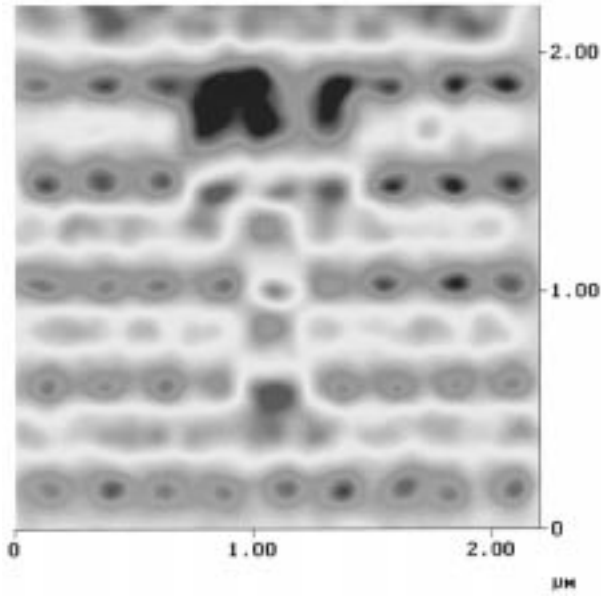

(a)

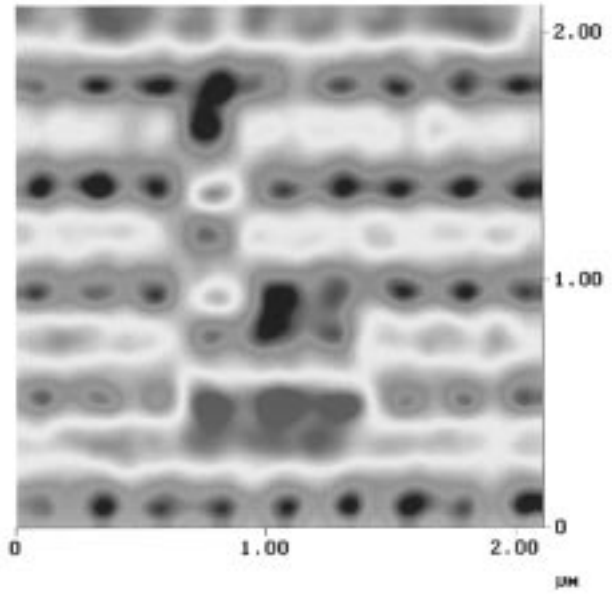

(b)

Fig. 24. Writing of a 7.5-Gb/in^2 longitudinal QMD using a MFM tip. The red represents attractive force between the tip and the sample and the blue repulsive force.

H. Overcome Superparamagnetic Limits

In a conventional disk, one bit is represented by approximately 1000 weakly coupled polycrystalline grains. In a QMD, each bit is stored in one discrete element which is exchangely isolated from other elements, but inside the element polycrystalline grains are strongly coupled by the exchange force, behaving more like a large single magnetic grain. Therefore, the volume and switching energy for the QMD elements are much greater than that of a single grain in a conventional disk, allowing significant reduction of bit

size without reaching the superparamagnetic limit. Finally, for a given material volume, a larger shape anisotropy in the QMD elements can lead to a larger switching field, allowing further increase data density [25].

I. Future Development of QMD's

It is clear that the QMD is a promising new paradigm to achieve a storage density of 0.5 Tb/in^2—several orders of magnitude higher than the limit of conventional magnetic disks. QMD's can be produced economically by imprint lithography. In fact, a 400-Gdots/in^2 array has been fabricated using nanoimprint lithography (Fig. 7). To overcome superparamagnetic limit, the shape anisotropy should be increased while keeping the diameter fixed. To be able to write and read, such a high-density, innovative ultra-high-resolution, high-speed write/read head and servo systems must be developed. One approach is the scanning probe-based technology, which is at present effective but too slow for a commercial disks. Currently, there are efforts in developing fast response scanning probe tips of a high bandwidth and parallel tip arrays [57], [58]. Before such write and read heads are developed, it is possible to use conventional heads to write and read a QMD, if multiple single-domain element per bit scheme is used. Finally, the future QMD disk drive itself could have linear rather than rotational motion. Because of ultra-high-density, a 100-Gb QMD media could have a size less than a penny. One should also expect such a disk drive to be low power and light weight.

VII. Transport in Nanoscale Magnetic Structures

Magnetoresistance in patterned magnetic nanostructures can be very different from that in a thin film or bulk material, because the magnetic domains in the PMN are very few and well defined, and can be precisely controlled by pattern's size and shape. Here, we present the transport in three intriguing systems.

A. Over 600% In-Plane-Hall Magnetoresistance Change in Micronscale Nickel Thin-Film Squares

Anisotropic magnetoresistance (AMR) in ferromagnetic thin films is typically 1%–2%. When measuring the MR change of a 4-mm-diameter Ni/Co multilayer disk by sending the current in the direction across the direction of the voltage, a 138% change was observed and it was attributed to the bridge effect in a distributed current flow. As the size of a ferromagnetic thin film square is reduced into micron scale, the magnetic domains in the square will change from random to ordered. This will have a profound effect on the MR change.

Fig. 25 shows that for a 2-μm square, the MR change, defined as $(R_{\max}-R_{\min})/R_{\min}$, is 610%, where the current (I) is driven across the two leads along a diagonal direction of a rectangle and the voltage (V) is measured at the other pair of leads in the other diagonal direction to obtain the resistance (V/I) [59]. An in-plane magnetic field is applied in parallel to a side of the rectangle. The average field

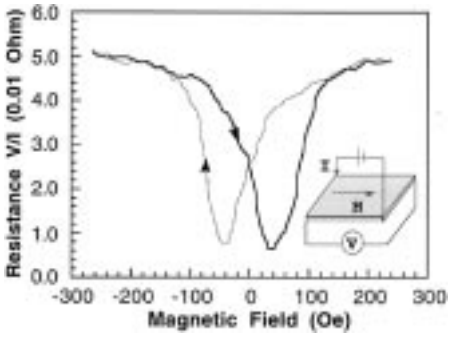

Fig. 25. Resistance V/I versus magnetic field. For a 2-μm square, the MR change, defined as $(R_{\max}-R_{\min})/R_{\min}$, is 610%, where the current (I) is driven across the two leads along a diagonal direction of a square and the voltage (V) is measured at the other pair of leads in the other diagonal direction to obtain the resistance (V/I).

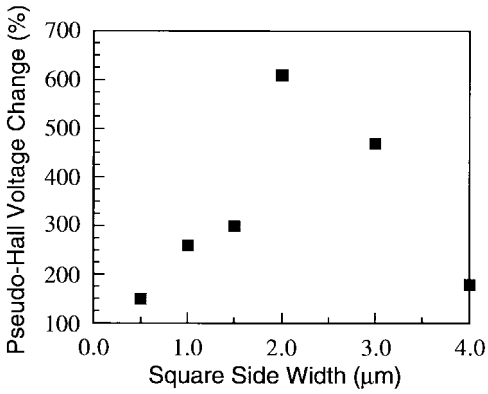

Fig. 26. Variation of the MR change as a function of the square width with the same magnetic field orientation as that in Fig. 25.

sensitivity for the cross configuration is 7% Oe^{-1} for a field range from −40 to 40 Oe.

Fig. 26 shows that the variation of the MR change as a function of the square width with the same magnetic field orientation as that in Fig. 25, indicating that although all square samples have a symmetrical shape, the MR change strongly depends on the actual size. The MR change for the Ni thin-film squares maximizes at 2-μm width. Larger or smaller than this width, the MR change will decrease.

Next, the importance of the shape symmetry of the rectangles is investigated and is found to be very critical to obtaining the extraordinary MR effect. The MR change as a function of length-to-width ratio of 1-μm-wide Ni thin-film rectangles is shown in Fig. 27. In our fabrication, the sample size and aspect ratio can be precisely controlled due to the use of high-resolution e-beam lithography. At unity aspect ratio, i.e., with 1-μm-sized squares, 260% of MR change has been observed. For a 2% deviation of the aspect ratio from unity, as presented in Fig. 27, the MR drops to 20%, representing an order of magnitude drop.

Magnetic force microscopy (MFM) has been used to study the magnetic domain structures of the samples. It is found that in the 2-μm squares where the in-plane-Hall MR

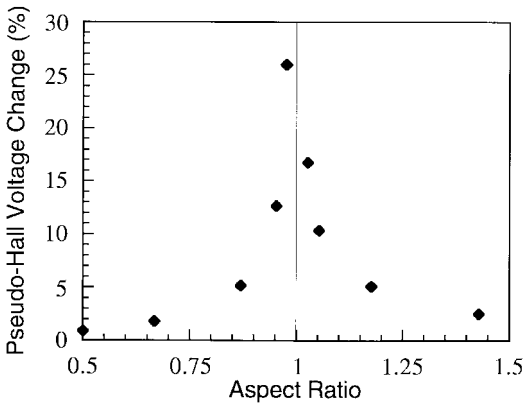

Fig. 27. MR change as a function of length-to-width ratio of 1-μm-wide Ni thin-film rectangles.

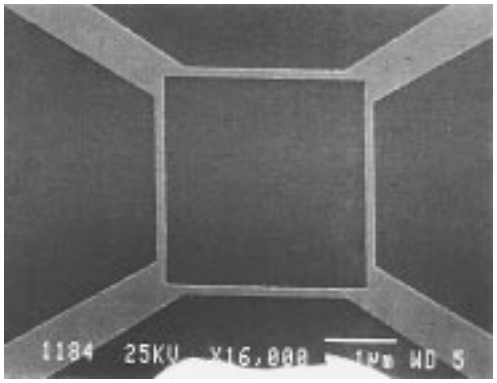

Fig. 28. The SEM image of a Ni frame with voltage/current leads at the corners. The frame's bar width is 100 nm and length is 3 μm.

change is over 600%, the MFM image consists of four well-defined symmetrical closure domains with identical shape and four 90° domain walls. For the squares of a 1-μm width or less, the MFM image shows a single domain with a north pole and a south pole and the magnetization direction in the diagonal of the square. For the squares of 3-μm width, the MFM image shows a chaos domain pattern. The MFM study indicated that the large MR change can be attributed to the well-defined symmetrical magnetic domain formation in the micronscale Ni film.

B. Nanoscale Single-Domain Magnetoresistive Bridge Sensor

Conventional magnetoresistive (MR) bridge sensors require magnetic bias fields to linearize the MR response, and occupy large area, typically 200 μm $\times$ 200 μm [60], [61]. Recently, we proposed [62] and demonstrated [63] a new MR bridge sensor that is based on the properties of single-domain nanostructures. It no longer requires any biasing field and occupies only 3 μm $\times$ 3 μm area, and therefore is suitable for mapping two-dimensional field distribution with ultra-high spatial resolution.

The nanoscale single-domain magnetoresistive (NSM) bridge sensor has a ferromagnetic frame with each bar (e.g., 100-nm width and 3-μm length) acting as one of the four resistors of a bridge (Fig. 28). Because of a small size and large shape anisotropy, each bar becomes a single domain without any external field. Therefore, in zero external field, the bridge is well balanced without a biasing field. Furthermore, our study has shown that the difference between the transverse and longitudinal MR of a single domain bar is very large, since it has near zero longitudinal MR. The NSM bridge was fabricated using electron beam lithography and lift-off.

Room-temperature MR measurements of the NSM sensor were performed with a constant current (less than 10 μA to avoid heating) passing through two leads along a diagonal direction of the frame and the voltage difference between the other two leads measured as the sensor output (Fig. 29). The resistance is defined as the ratio of the voltage to the current. The magnetic field was applied in the plane of the

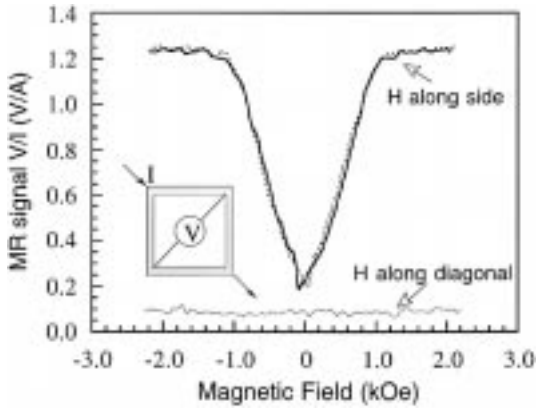

Fig. 29. The MR response of the Ni frame of 3-μm bar length and 100-nm width. The field direction is along the frame side for the upper curve and along the diagonal for the lower curve. The dotted line represents a forward scan of the field and the solid line represents a backward scan. Shown in the inset is the MR measurement configuration.

frame. At zero external field, the sensor has a very small offset. Between zero and the saturation field (1 kOe), the sensor output has a good linearity and little hysteresis.

MR response curves of the frame MR sensor are shown in Fig. 29. When applying the field along a frame side, the sensor output increases with the field strength and a good linearity of MR response can be seen within a large range between zero and the saturation field (1 kOe). The near-zero offset and good linearity in the sensor response are attributed to 1) the excellent symmetrical shape of the frame controlled by the fabrication; 2) single domain formation in each bar; 3) the biasing field created by neighboring single-domain bars that further enforces a single-domain; and 4) the spin rotation process dominating the magnetization reversal.

The field orientation dependence of the sensor output has been measured (Figs. 29 and 30). When the field direction is along the diagonal of the frame, all the four resistors have the same resistance regardless the field strength, leading to a balanced bridge and near zero output. When the external field is above the saturation field, the output is nearly linear with the field angle; below the saturation field, it is less linear.

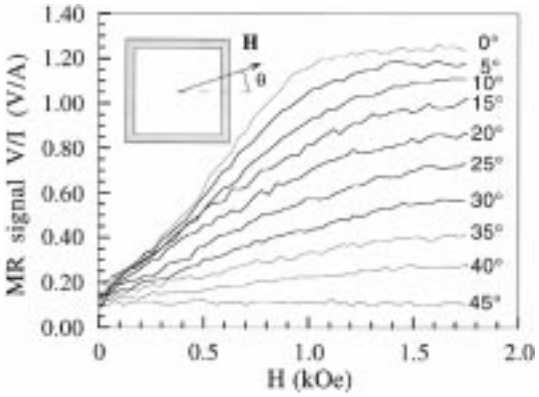

Fig. 30. The field orientation dependence of the MR response of the Ni frame sensor. The angle θ is between the field direction and the frame side.

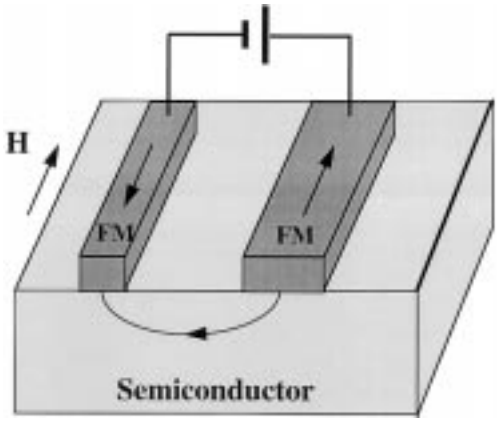

Fig. 31. Schematic of FM/S/FM diode.

C. Spin Valve Effects in Nickel/Silicon/Nickel Diodes

Another application of the PMN in sensors is the FM/S/FM diode, which has two sets of interdigited nanofingers on top of a silicon substrate [64]. Each set of fingers has 35-nm thickness, 14-mm length, but different finger width and therefore different switching field, as shown in Fig. 31 [65].

In MR measurements, a small ac voltage signal (40 mV) was applied to the diode and the differential resistance was measured using a lock-in amplifier. For the devices with a finger width of 75 nm for one set and 150 nm for the other, the resistance as a function of the in-plane magnetic field applied parallel along the finger length is shown in Fig. 32. For a forward scan of the magnetic field from -600 Oe, the resistance has a sharp increase around -50 Oe, stays flat and then a sharp decrease around 380 Oe. The amplitude of MR change was typically $0.3 \sim 0.6\%$ at room temperature but somewhat increased with lower temperatures. Furthermore, such MR changes were not observed for the FM/S/FM diodes with identical finger widths.

The above observed effect can be explained using a spin-valve model: the resistance depends on the relative spin orientation of the two FM finger sets. Since the two finger sets have different switching fields, at certain magnetic field range, the two sets of fingers have anti-parallel spin orientation, therefore a higher resistance. In the other region, the spins of two finger sets are parallel to each other, which results in a lower resistance.

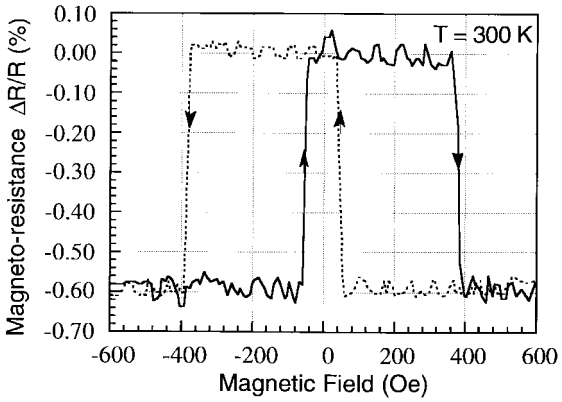

Fig. 32. Resistance as a function of the in-plane magnetic field applied parallel along the finger length for the devices with a finger width of 75 nm for one set and 150 nm for the other.

The finger spacing of the devices is typically 500 nm; hence, tunneling is very unlikely. In fact, the current is dominated by the thermionic emission across the schottky barrier. One explanation for the spin valve effects is the spin-dependent scattering at the interface and inside of the ferromagnetic fingers. Other explanations are being considered and further investigation is underway.

VIII. Other Applications of Nanoscale Patterning in Magnetics

Besides those discussed above, nanostructures can impact magnetic research and developments in many other ways. Two examples are given here. One is an ultra-high resolution MFM tip. Conventionally, MFM tips are either sharpened Fe wires [66] or magnetically coated atomic force microscope tips [67]. Both kinds of tips suffer from several drawbacks. First, the tips are large in area and consist of multiple magnetic domains, therefore having a broad distribution of magnetic charge, which results in poor spatial resolution. Second, the tips have a sizable magnetic charge that can alter the magnetic properties of the magnetic material under inspection. To avoid such interference, the tip has to be kept rather far away from the sample surface, drastically reducing the MFM's sensitivity.

In 1993, we demonstrated a new, ultra-small, single-domain MFM tip that has very small magnetic charges and offers a spatial resolution and sensitivity many times greater than other MFM tips [14]. The new MFM tip consists of a nonmagnetic pillar $\sim$150 nm in diameter and over 1-μm long on the apex of a commercial AFM tip, and a pointed magnetic spike 30-nm thick, about 150-nm wide, and over 1-μm long coated on one side of the pillar (Fig. 33). The nonmagnetic pillar was fabricated by contamination e-beam lithography and the magnetic needle was produced using a shadow evaporation of nickel. Simulation shows the spike tip has a much higher spatial resolution (Fig. 34) and a much smaller stray field (Fig. 35) than conventional tips.

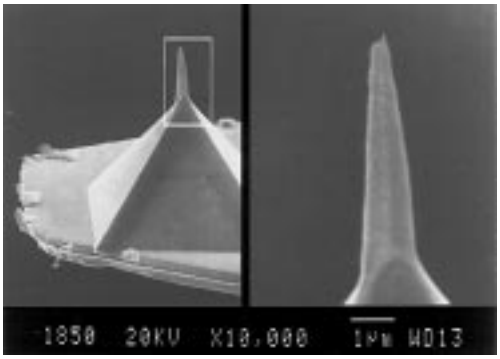

Fig. 33. SEM image of a spike MFM tip.

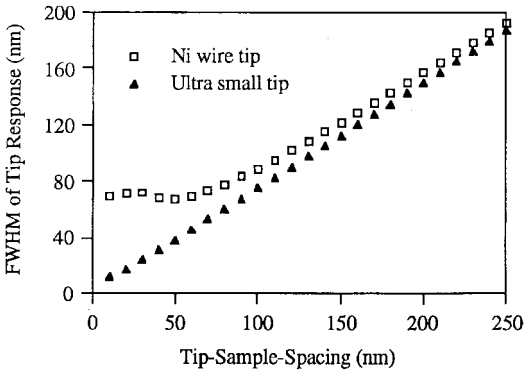

Fig. 34. FWHM response of the spike and Ni wire tips to a magnetic dipole for different values of tip-to-sample spacing.

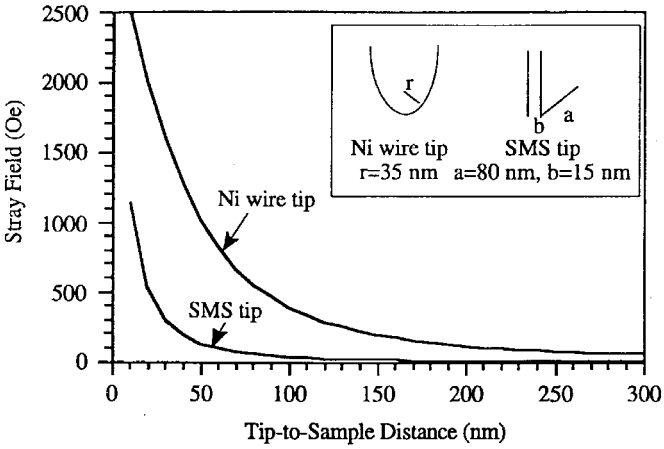

Fig. 35. Stray field of spike and Ni tips.

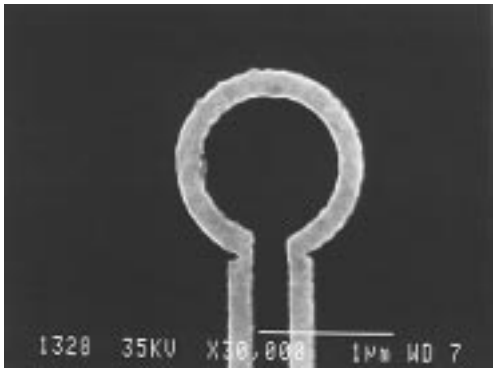

Fig. 36. SEM image of a ring with an inner diameter of 1 μm and a width of 200 nm.

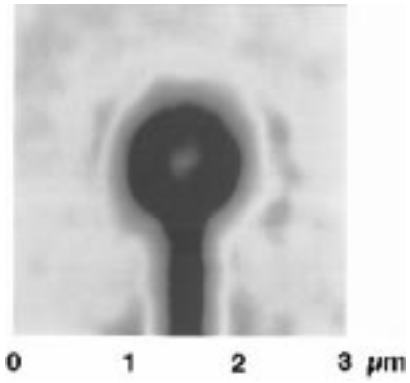

(a)

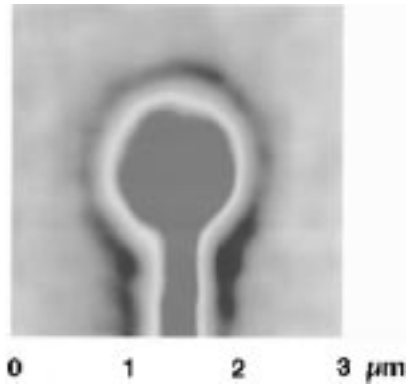

(b)

Fig. 37. MFM image of the same ring shown in Fig. 36 when current $I = \pm 3$ mA. The background is zero magnetic force and the red area represents attractive magnetic force. The current direction in (b) is opposite from that in (a).

The spike tip was used to image 7.5-Gb/in^2 QMD (Fig. 7) and showed much superior spatial resolution than that of a conventional MFM tip.

The second example is the quantification of magnetic force microscopy using nanoscale current rings [68]. Scanning-probe based MFM is an essential tool for characterizing magnetic materials in submicron scale. To quantitatively interpret the MFM signal is very challenging, because the exact magnetic properties of a MFM tip are generally unknown [69]–[73]. We show a method using nanoscale current rings to calibrate MFM probes. The metal rings with an inner diameter of 1 or 5 μm and a width of 200 nm were fabricated using electron-beam lithography and a lift-off technique, as shown in Fig. 36. A current supplied by a precision current source passed through the ring via two wire leads. Fig. 37 shows the MFM images of the ring with an inner diameter of 1 μm when $I = \pm 3$ mA, respectively. The response signal of the MFM at the ring center varies nearly linearly with the current, shown in Fig. 38, suggesting that the MFM tip magnetization stays constant when the magnetic field from the ring increases.

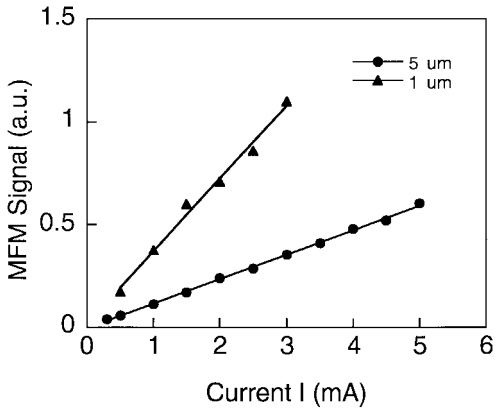

Fig. 38. Phase shift f of MFM versus current I in the ring with an inner diameter of 1 and 5 μm using the tip with 65-nm-thick Co film, showing a nearly linear relation.

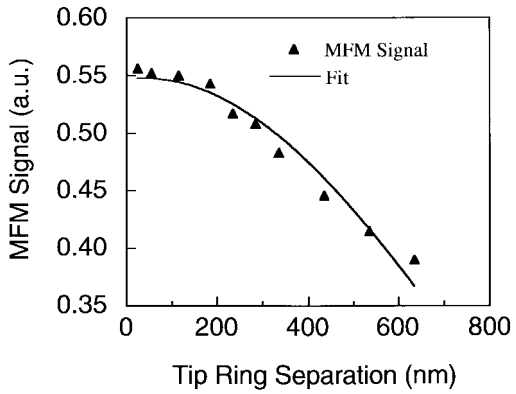

Fig. 39. MFM signal at the ring center verus the tip-ring separation for the ring with an inner diameter of 5 μm and a current of 5 mA using the tip with 65-nm-thick Co film. The triangles represent the experimental data and the solid line is the fitting result.

The characteristics can be investigated by fitting the MFM signal as a function of the distance between the tip and the ring, as shown in Fig. 39. The effective magnetic charge, q, and the effective magnetic moment, m_z, of a MFM tip with 65-nm-thick Co film are determined to be 2.8 $\times$ 10^{-6} emu/cm and 3.8 $\times$ 10^{-9} emu, respectively. The measurement using a straight current wire shows that the m_x and m_y are three orders of magnitude smaller than m_z. From the minimum detectable loop current in Fig. 38, the tip's sensitivity to the second derivative of the magnetic field is found to be about 0.1 Oe/nm^2.

IX. Conclusion

Using nanolithography-based fabrication technology, magnetic structures can be engineered to have properties that cannot be achieved by conventional methods. Undoubtedly, the nanofabrication approach opens up new opportunities for engineering novel magnetic materials, understanding the fundamentals of magnetics, exploring limits of magnetic storage, and developing ultra-high-density magnetic storage, innovative read and write heads, magnetotransport devices, and magnetooptical devices.

Acknowledgment

The author would like to thank the people who have contributed significantly to the results reviewed in the paper. In particular, Prof. J.-G. Zhu, who introduced the author to magnetic nanostructures; Dr. L. Cooper, whose enthusiasm and support are essential; P. R. Krauss for his substantial contributions in QMD fabrication, nanoimprint lithography and manuscript preparation; Dr. L. Kong for MFM measurements, MFM tip calibration and manuscript preparation; Dr. Y.-Q. Jia for transport measurements; U. Suriono for micromagnetics simulation; Dr. P. Fischer for MFM spike tip fabrication; M. Wei for single-domain elements; P. Renstrom for nanoimprint lithography; R. Guibord for fabrication; and other members of the NanoStructure Lab at the University of Minnesota.

References

[1] E. J. Ozimek, "Characteristic length of domain structures and its effect on the coercive force of ferromagnetic materials," *J. Appl. Phys.*, vol. 57, p. 5406, 1985.
[2] B. W. Corb, "Charging on the metastable domain states of small NiFe rectangles," *IEEE Trans. Magn.*, vol. MAG-24, p. 2386, 1988.
[3] D. S. Lo, G. J. Cosimini, L. J. Zierhut, R. H. Dean, and M. C. Paul, "A Y-domain magnetic thin film memory element," *IEEE Trans. Magn.*, vol. MAG-21, p. 1776, 1985.
[4] G. J. Cosimini, D. S. Lo, L. G. Zierhut, M. C. Paul, R. H. Dean, and K. J. Matysik, "Improved Y-domain magnetic film memory elements," *IEEE Trans. Magn.*, vol. MAG-24, p. 2060, 1988.
[5] M. Ruhrig, W. Bartsch, M. Vieth, and A. Hubert, "Elementary magnetization processes in a low-anisotropy circular thin film disk," *IEEE Trans. Magn.*, vol. MAG-26, p. 2807, 1990.
[6] H. A. M. v. d. Berg, "Domain structure in soft-ferromagnetic thin-film objects," *J. Appl. Phys.*, vol. 61, p. 4194, 1987.
[7] S. McVitie and J. N. Chapman, "Magnetic structure determination in small regularly shaped particle using transmission electron microscopy," *IEEE Trans. Magn.*, vol. MAG-24, p. 1778, 1988.
[8] J. N. Chapman, S. McVitie, and S. J. Hefferman, "Mapping induction distributions by transmission electron microscopy," *J. Appl. Phys.*, vol. 69, p. 6078, 1991.
[9] J. F. Smyth, S. Schultz, D. R. Fredkin, T. Koehler, I. R. McFaydlin, D. P. Kern, and S. A. Rishton, "Hysteresis of submicron permalloy particulate arrays," *J. Appl. Phys.*, vol. 63, p. 4237, 1988.
[10] G. A. Gibson, J. F. Smyth, S. Schultz, and D. P. Kern, "Observation of the switching fields of individual Permalloy particles in nanolithographic arrays via magnetic force microscopy," *IEEE Trans. Magn.*, vol. MAG-27, p. 5187, 1991.
[11] G. A. Gibson and S. Schultz, "Magnetic force microscope study of the micromagnetics of submicrometer magnetic particles," *J. Appl. Phys.*, vol. 73, p. 4516, 1993.
[12] M. Lederman, G. A. Gibson, and S. Schultz, "Observation of thermal switching of a single ferromagnetic particle," *J. Appl. Phys.*, vol. 73, p. 6961, 1993.
[13] T. Chang, M. Lagerquist, J. G. Zhu, J. H. Judy, P. B. Fisher, and S. Y. Chou, "Deconvolution of magnetic force images by Fourier analysis," *IEEE Trans., Magn.* vol. 28, p. 3138, 1992.
[14] P. B. Fischer, M. S. Wei, and S. Y. Chou, "Ultrahigh resolution magnetic force microscope tip fabricated using electron beam lithography," *J. Vac. Sci. Tech. B*, vol. 11, p. 2570, 1993.
[15] S. Y. Chou, M. S. Wei, P. R. Krauss, and P. B. Fischer, "Single-domain magnetic pillar array of 35 nm diameter and 65 Gbits/in density for ultrahigh density quantum magnetic storage," *J. Appl. Phys.*, vol. 76, p. 6673, 1994.
[16] ——, "Study of nanoscale magnetic structures fabricated using electron-beam lithography and quantum magnetic disk," *J. Vac. Sci. Tech. B*, vol. 12, p. 3695, 1994.

[17] P. R. Krauss, P. B. Fischer, and S. Y. Chou, "Fabrication of single-domain magnetic pillar array of 35 nm diameter and 65 Gbits/in^2 density," *J. Vac. Sci. Tech. B*, vol. 12, p. 3639, 1994.
[18] S. Y. Chou, P. R. Krauss, and P. Renstrom, "Imprint of sub-25 nm vias and trenches in polymers,"*Appl. Phys. Lett.*, vol. 67, p. 3113, 1995.
[19] ——, "Imprint lithography with 25-nanometer resolution," *Science*, vol. 272, p. 85, 1996.
[20] R. M. H. New, R. F. W. Pease, and R. L. White, "Submicron patterning of thin cobalt films for magnetic storage," *J. Vac. Sci. Tech. B*, vol. 12, p. 3196, 1994.
[21] ——, "Physical and magnetic properties of submicron lithographically patterned magnetic islands," *J. Vac. Sci. Tech. B*, vol. 13, p. 1089, 1995.
[22] R. M. H. New, R. F. W. Pease, R. L. White, R. M. Osgood, and K. Babcock, "Effect of magnetocrystalline anisotropy in single-domain polycrystalline cobalt islands," *IEEE Trans. Magn.*, vol. 31, p. 3805, 1995.
[23] ——, "Magnetic force microscopy of single-domain single-crystal iron particles with uniaxial surface anisotropy,"*J. Appl. Phys.*, vol. 79, p. 5851, 1996.
[24] S. Y. Chou and P. B. Fischer, "Double 15-nm-wide metal gates 10 nm apart and 70 nm thick on GaAs," *J. Vac. Sci. Tech. B*, vol. 8, p. 1919, 1990.
[25] B. D. Cullity, *Introduction to Magnetic Materials*. Reading, MA: Addison-Wesley, 1972.
[26] L. Kong and Y. S. Chou, "Effects of bar length on switching field of nanoscale nickel and cobalt bars fabricated using lithography," *J. Appl. Phys.*, vol. 80, p. 5205, 1996.
[27] J. F. Smyth, S. Schultz, D. R. Fredkin, D. P. Kern, S. A. Rishton, H. Schmid, M. Cali, and T. R. Koehler, "Hysteresis in lithographic arrays of Permalloy particles: Experiment and theory," *J. Appl. Phys.*, vol. p. 5262, 1991.
[28] E. C. Stoner and E. P. Wohlfarth, "A mechanism of magnetic hysteresis in heterogeneous alloys," *Philos. Trans. R. Soc. A*, vol. 240, p. 599, 1948.
[29] H. Mutoh, K. Kanai, I. Okamoto, Y. Ohtsuka, T. Sugawara, J. Koshikawa, J. Toda, Y. Uematsu, M. Shinohara, and Y. Mizoshita, "5 Gb/in^2 recording demonstration with NiFe/Co_{90}/Fe/$_{10}$ spin-valve heads and low-noise thin-film disks," in *IEEE Int. Magn. Conf.*, Seattle, WA, 1996.
[30] M. H. Kryder, W. Messner, and L. R. Carley, "Approaches to 10 Gbit/in^2 recording," *J. Appl. Phys.*, vol. 79, p. 4485, 1996.
[31] J. A. Brug, L. Tran, M. Bhattacharyya, A. Jander, J. H. Nickel, and T. C. Anthony, "Impact of new magnetoresistive materials on magnetic recording heads," *J. Appl. Phys.*, vol. 79, p. 4491, 1996.
[32] D. N. Lambeth, E. M. T. Velu, G. H. Bellesis, L. L. Lee, and D. E. Laughlin, "Media for 10 Gb/in^2 hard disk storage: Issues and status," *J. Appl. Phys.*, vol. 79, p. 4496, 1996.
[33] K. D. Fisher and C. S. Modlin, "Signal processing for 10 GB/in^2 magnetic disk recording and beyond," *J. Appl. Phys.*, vol. 79, p. 4502, 1996.
[34] B. Maron, "Head/disk tribology: Toward 10 Gb/in^2," *J. Appl. Phys.*, vol. 79, p. 4508, 1996.
[35] C. Kittle, J. K. Galt, and W. E. Campell, "Crucial experiment demonstrating single domain properties of fine ferromagnetic powders," *Phys. Rev.*, vol. 77, p. 725, 1950.
[36] A. Aharoni, "Perfect and imperfect particles," *IEEE Trans. Magn.*, vol. MAG-22, p. 478, 1986.
[37] ——, "Upper bound to a single-domain behavior of a ferromagnetic cylinder," *J. Appl. Phys.*, vol. 68, p. 2892, 1990.
[38] ——, "The concept of a single-domain particle," *IEEE Trans. Magn.*, vol. 27, p. 4775, 1991.
[39] P. B. Fischer and S. Y. Chou, "10 nm electron beam lithography and sub-50 nm overlay using a modified scanning electron microscope," *Appl. Phys. Lett.*, vol. 62, p. 2989, 1993.
[40] P. B. Fischer, K. Dai, E. Chen, and S. Y. Chou, "10 nm Si pillars fabricated using electron-beam lithography, reactive ion etching, and HF etching," *J. Vac. Sci. Tech. B*, vol. 11, p. 2524, 1993.
[41] L. F. Shew, "Discrete tracks for saturation magnetic recording," *IEEE Trans., BTR*, vol. 9, p. 56, 1963.
[42] S. E. Lambert, I. L. Sander, A. M. Patlach, and M. T Krounbi, "Recording characteristics of submicron discrete magneti tracks," *IEEE Trans. Magn.*, vol. MAG-23, p. 3690, 1987.
[43] K. A. Belser, T. Makansi, and I. L. Sanders, U.S. Patent no. 4 912 585, Mar. 1990.
[44] S. E. Lamber, I. L. Sanders, A. M. Pattan, M. T. Krounbi, and S. R. Hetzler, "Beyond discrete tracks: Other aspects of patterned media," *J. Appl. Phys.*, vol. 69, p. 4724, 1991.
[45] S. Y. Chou, P. R. Krauss, and L. Kong, "Nanolithographically defined magnetic structures and quantum magnetic disk," *J. Appl. Phys.*, vol. 79, p. 6101, 1996.
[46] P. R. Krauss and S. Y. Chou, "Fabrication of planar quantum magnetic disk structure using electron beam lithography, reactive ion etching, and chemical mechanical polishing," *J. Vac. Sci. Tech. B*, vol. 13, p. 2850, 1995.
[47] L. Kong, L. Zhuang, and S. Y. Chou, "Writing of 7.5 Gbits/in2 longitudinal quantized magnetic disks using magnetic froce microscope," in *Proc. IEEE Int. Magn. Conf.*, New Orleans, LA, 1997.
[48] U. Suriono and S. Y. Chou, unpublished.
[49] J. W. F. Brown and A. E. Labonte, "The fundamental theorem of fine-ferromagnetic-particle theory," *J. Appl. Phys.*, vol. 36, p. 1380, 1965.
[50] A. E. LaBonte, "The fundamental theorem of the theory of fine ferromagnetic particles," *J. Appl. Phys.*, vol. 40, p. 2450, 1969.
[51] S. W. Yuan and H. N. Bertram, "Domain-wall dynamic transitions in thin films," *Phys. Rev. B*, vol. 44, p. 12395, 1991.
[52] D. V. Berkov, K. Ramstock, and A. Hubert, "Solving micromagnetic problems. Towards an optimal numerical method," *Phys. Stat. Sol. (a)*, vol. 137, p. 207, 1993.
[53] S. Muller-Pfeiffer, M. Schneider, and W. Zinn, "Imaging of magnetic domain walls in iron with a magnetic force microscope: A numerical study," *Phys. Rev. B*, vol. 49, p. 15745, 1994.
[54] S. W. Yuan and H. N. Bertram, "Fast adaptive algorithms for micromagnetics," *IEEE Trans. Magn.*, vol. 25, p. 2031, 1992.
[55] R. H. Victora, "Micromagnetic predictions for magnetization reversal in CoNi films," *J. Appl. Phys.*, vol. 62, p. 4220, 1987.
[56] M. E. Schabes and H. N. Bertam, "Magnetization processes in ferromagnetic cubes," *J. Appl. Phys.*, vol. 64, p. 1347, 1988.
[57] S. R. Manalis, S. C. Minne, A. Atalar, and C. F. Quate, "High-speed atomic force microscopy using an integrated actuator and optical lever detection," *Rev. Scientific Instruments*, p. 3294, 1996.
[58] H. J. Mamin, B. D. Terris, L. S. Fan, S. Hoen, R. C. Barrett, and D. Rugar, "High-density data storage using proximal probe techniques," *IBM J. Res. Develop.*, vol. 39, p. 681, 1995.
[59] Y. Q. Jia, R. C. Shi, and S. Y. Chou, "Observation of 600% magnetoresistance change in micron-scale nickel structures," in *IEEE Proc. Int. Magn. Conf.*, Seattle, WA, 1996.
[60] U. Dibrell and A. Peterson, *Elec. Comp.*, vol. APPL-5, p. 148, 1983.
[61] J. M. Daughton, J. Brown, E. Chen, R. Beech, A. Pohm, and K. Kude, "Magnetic field sensors using GMR multilayer," *IEEE Trans. Magn.*, vol. MAG-30, p. 4608, 1994.
[62] S. Y. Chou, private communication, p. 1995.
[63] Y. Jia, L. Zhuang, and S. Y. Chou, "A nanoscale single-domain magnetoresistance bridge sensor," in *IEEE Int. Magn. Conf.*, New Orleans, LA, 1997.
[64] Y. Q. Jia, R. C. Shi, and S. Y. Chou, "Spin-valve effects in nickel/silicon/nickel junctions," *IEEE Trans. Magn.*, vol. 32, p. 4707, 1996.
[65] M. S. Wei and S. Y. Chou, "Size effects on switching field of isolated and interactive arrays of nanoscale single-domain Ni bars fabricated using electron-beam nanolithography," *J. Appl. Phys.*, vol. 76, p. 6679, 1994.
[66] Y. Martin and H. K. Wickramsinghe, "Magnetic imaging by force microscopy with 1000 A resolution," *Appl. Phys. Lett.*, vol. 50, p. 1455, 1987.
[67] Y. Honda, S. Hosaka, A. Kikugawa, S. Tanaka, Y. Matsuda, M. Suzuki, and M. Futamoto, "A magnetic force microscope using an optical lever sensor and its application to longitudinal recording media," *Jpn. J. Appl. Phys.*, vol. 31, p. L1061, 1992.

[68] L. Kong and S. Y. Chou, "Qunatification of magnetic force microscopy using a micronscale current ring," in *Proc. 41st Ann. Conf. Magnetism Magn. Mat.*, Atlanta, GA, 1996.
[69] D. Rugar, H. J. Mamin, P. Guethner, S. E. Lambert, J. E. Stern, I. McFadyen, and T. Yogi, "Magnetic force microscopy: General principles and application to longitudinal recording media," *J. Appl. Phys.*, vol. 68, p. 1169, 1990.
[70] K. Babcock, V. Elings, M. Dugas, and S. Loper, "Optimization of thin-film tips for magnetic force microscopy," *IEEE Trans. Magn.*, vol. 30, p. 4503, 1994.
[71] R. B. Proksch, S. Foss, and E. D. Dahlberg, "High resolution magnetic force microscopy of domain wall fine structures," *IEEE Trans. Magn.*, vol. 30, p. 4467, 1994.
[72] T. Goddenhenrich, H. Lemke, M. Muck, U. Hartmann, and C. Heiden, "Probe calibration in magnetic force microscopy," *Appl. Phys. Lett.*, vol. 57, p. 2612, 1990.
[73] R. B. Proksch, T. E. Schaffer, B. M. Moskowitz, E. D. Dahlberg, D. A. Bazylinski, and R. B. Frankel, "Magnetic force microscopy of the submicron magnetic assembly in a magnetotactic bacterium," *Appl. Phys. Lett.*, vol. 66, p. 2582, 1995.

Stephen Y. Chou received the Ph.D. degree from the Massachusetts Institute of Technology, Cambridge, in 1986.

In the same year, he joined Stanford University, Stanford, CA, first as a Research Associate, then a Lecturer, and later an Acting Assistant Professor with the Department of Electrical Engineering. In 1989, he joined the University of Minnesota, Minneapolis, as an Assistant Professor, and he became an Associate Professor in 1992 and a Professor in 1994. His current research focuses on developing and exploring 1) new nanotechnologies that will fabricate structures and devices substantially smaller and cheaper than current technology permits and 2) innovative nanoscale electronic, optoelectronic, and magnetic devices by combining cutting-edge nanotechnology with frontier knowledge from different disciplines. He has published more than 120 journal and conference papers.

Dr. Chou has received McKnight-Land Grant Professor, Packard Fellow, the University of Minnesota's George Taylor Distinguished Research Award, and an IBM Faculty Development Award.